Existence and uniqueness in ocean-atmosphere turbulent flux algorithms in E3SM

Justin Dong[1], Michael A. Brunke[2], Xubin Zeng[2], Carol S. Woodward[1], Christopher J. Vogl[1], Hui Wan[3]

[1]Center for Applied Scientific Computing, Lawrence Livermore National Laboratory
[2]Hydrology and Atmospheric Sciences, University of Arizona
[3]Atmospheric, Climate, and Earth Sciences Division, Pacific Northwest National Laboratory

Key Points:

- The equations underlying an ocean-atmosphere turbulent flux algorithm may have no solution or multiple solutions.
- Lack of a solution is caused by discontinuities in exchange coefficients and can be mitigated by regularizing discontinuities.
- Turbulent flux parameterizations can yield non-unique surface fluxes. *Ad hoc* stability limiters in E3SM can dictate when fluxes are unique.

Corresponding author: Justin Dong, `dong9@llnl.gov`

Abstract

We investigate whether or not the default ocean-atmosphere turbulent flux algorithm in the Energy Exascale Earth System Model version 2 (E3SMv2) converges to unique surface fluxes. We demonstrate that under certain conditions (i) discontinuities in the underlying equations result in the lack of a solution for the algorithm to converge to, and (ii) more than one set of surface fluxes may satisfy the aforementioned equations, some of which may have non-physical interpretation. These issues underpinning the theoretical foundations of the parameterization have significant impacts on the accuracy and convergence of turbulent fluxes in E3SM.

We address issues of non-existence and non-uniqueness of surface fluxes in E3SM's default algorithm by (a) regularizing discontinuous exchange coefficients to enforce continuity and allow the algorithm to converge to a solution of the underlying equations, and (b) utilizing an adaptive procedure for selecting limiting values of the Monin-Obukhov length to ensure the underlying equations have a unique solution. The proposed revisions result in significant changes to model latent and sensible heat fluxes which are most notable in boreal winter in the Northern Hemisphere.

Plain Language Summary

The ability of Earth system models to provide accurate predictions of climatological phenomena depends in part on accurately modeling interactions of the Earth's atmosphere and oceans. These interactions are encompassed by surface fluxes which represent the exchange of heat and momentum between the Earth's atmosphere and oceans. This work focuses on a set of equations commonly utilized in Earth system models such as the Energy Exascale Earth System Model version 2 (E3SMv2) to compute ocean-atmosphere surface fluxes and demonstrates that under certain circumstances, these equations can have no solution or more than one solution. The currently used formulation for solving these equations in E3SM has no safeguards in place for detecting when these undesired scenarios occur and thus returns non-physical solutions with large residual errors in these scenarios. We propose several modifications to this formulation for solving these ocean-atmosphere interaction equations in E3SM which ensure that a unique solution exists, thereby improving accuracy of the surface fluxes and ensuring interpretability of the surface flux algorithms.

1 Introduction

An accurate calculation of ocean-atmosphere surface fluxes, which affect both the atmosphere and the ocean, is crucial to Earth system modeling. Since such fluxes occur at spatial and temporal scales that are much smaller than those of a typical Earth system model (ESM) grid cell ($\sim 1^\circ \times 1^\circ$), surface turbulent flux algorithms are employed to relate these fluxes to the large-scale mean quantities (lowest atmospheric layer wind speed, temperature, and specific humidity, as well as sea surface temperature) that are resolved dynamically. Generally, surface wind stress (τ), sensible heat flux (SH), and latent heat flux (LH) are related to these mean quantities thusly (Brunke et al., 2002, 2003):

$$\tau = \rho_a C_D S U, \qquad \mathrm{SH} = \rho_a C_p C_H S(\theta_s - \theta_a), \qquad \mathrm{LH} = \rho_a L_v C_E S(q_s - q_a), \tag{1}$$

where ρ_a is air density; C_p is the specific heat of air; L_v is the latent heat of vaporization; U is the wind speed; S is the wind speed plus wind gustiness if considered ($S = U$ if it is not considered); θ_s is the sea surface potential temperature; θ_a is the potential temperature of the lowest layer of the atmosphere model; q_s is the sea surface specific humidity; q_a is the lowest atmosphere model layer specific humidity; and C_D, C_H, and C_E are the turbulent exchange coefficients for momentum, heat, and humidity, respectively.

Through Monin-Obukhov similarity theory (MOST) (Monin & Obukhov, 1954), one may derive alternative expressions for the exchange coefficients which are dependent on scaling parameters, u_*, θ_*, and q_*:

$$C_D = \frac{u_*^2}{SU}, \qquad C_H = -\frac{u_*\theta_*}{S(\theta_s - \theta_a)}, \qquad C_E = -\frac{u_* q_*}{S(q_s - q_a)}. \tag{2}$$

The surface wind stress and sensible and latent heat fluxes may then be expressed as

$$\tau = \rho_a u_*^2, \qquad \mathrm{SH} = -\rho_a C_p u_* \theta_*, \qquad \mathrm{LH} = -\rho_a L_v u_* q_*. \tag{3}$$

The scaling parameters u_*, θ_*, and q_* must be determined iteratively since they are implicitly defined using stability functions that account for the effect of convective (in)stability on vertical fluxes. These stability functions are dependent on the stability parameter ζ which is a function of the scaling parameters and defined by

$$\zeta(u_*, \theta_*, q_*) = z/L(u_*, \theta_*, q_*), \tag{4}$$

where z is the height above the surface and L is the Monin-Obukhov length

$$L(u_*, \theta_*, q_*) = \frac{u_*^2 \theta_v}{kg\theta_{v*}(\theta_*, q_*)}.$$

Here, θ_v is the virtual potential temperature such that $\theta_v = \theta_a(1 + 0.61q_a)$ and θ_{v*} is the virtual potential temperature scaling parameter defined as $\theta_{v*}(\theta_*, q_*) = \theta_*(1 + 0.61q_a) + 0.61\theta_a q_*$. The constants k and g denote the von Kármán constant and standard acceleration of gravity, respectively.

All ocean-atmosphere turbulent flux parameterizations are based on either (1) or (3). However, there are key differences in assumptions underlying such parameterizations, for instance the range of surface conditions for which the parameterization is valid, whether wind gustiness is included, and whether a 2% reduction in humidity saturation at the ocean surface is assumed (Zeng et al., 1998; Brunke et al., 2002, 2003). A number of studies have quantified sensitivities of Earth system models to ocean-surface flux calculations (Harrop et al., 2018; W. G. Large & Caron, 2015; Zeng & Beljaars, 2005) as well as sensitivities to the choice of turbulent flux parameterization (Reeves Eyre et al., 2021).

Underpinning much of the prior analysis of turbulent flux parameterizations is the assumption that they are *well-posed*, that is, the underlying equations associated with the parameterization can be solved to obtain unique scaling parameters and surface fluxes. To the best of our knowledge, there has been no systematic analysis carried out to ascertain whether or not the aforementioned parameterizations can actually be solved uniquely for the surface fluxes. Instead, in many Earth system models, numerical methods are applied indiscriminately to approximate the surface fluxes without consideration of whether or not the approximated quantities actually satisfy the underlying equations.

In this study, we establish basic results on well-posedness, or lack thereof, for a particular ocean-atmosphere turbulent flux parameterization. We consider the default ocean-atmosphere turbulent flux parameterization based on the work of W. Large & Pond (1982) in the Energy Exascale Earth System Model version 2 (E3SMv2) (Golaz et al., 2019) but also discuss where the analysis in the present work applies to other turbulent flux algorithms as well. The aim of this study is to establish:

1. Whether or not there always exists a solution to the equations underlying the W. Large & Pond (1982) turbulent flux parameterization. We demonstrate that lack of solution existence is an issue that occurs in this parameterization due to discontinuities of some exchange coefficients. In this scenario, the computed surface fluxes introduce large errors that are then propagated into the ocean and atmosphere models.

2. Whether or not a solution to the equations underlying the turbulent flux parameterization (if it exists) is unique. We demonstrate that under certain atmospheric conditions there are multiple surface fluxes which satisfy the aforementioned equations, some of which have a non-physical interpretation. Moreover, the default E3SM parameterization may converge to these non-physical surface fluxes under certain circumstances, thereby introducing significant approximation error which is again propagated to the ocean and atmosphere models. We also demonstrate that the number of surface fluxes satisfying the underlying turbulent flux parameterization is strongly influenced by *ad hoc* limiters utilized in E3SM to restrict the Monin-Obukhov length to a desired range.

The analysis in this work is substantiated with model runs from E3SMv2 which demonstrate how these mathematical issues manifest in practice. Based on our analysis, we present several techniques to ensure that the turbulent flux parameterization is well-posed. These include regularization techniques to address discontinuous coefficients that prevent solution existence and an adaptive adjustment to Monin-Obukhov length limiters to ensure solution uniqueness.

The rest of this work is presented as follows. In Section 2, we provide an overview of ocean-atmosphere surface flux algorithms in E3SMv2. In Section 3 we analyze issues of well-posedness in the aforementioned algorithms and prescribe modifications to ensure well-posedness. Section 4 includes a sensitivity analysis of E3SM to the proposed modifications, followed by conclusions in Section 5.

2 Methodology

In this section, we describe the default ocean-atmosphere turbulent flux parameterization in E3SM and the numerical methods used to compute the turbulent fluxes. An analysis of the lack of mathematical well-posedness of the turbulent flux parameterization is presented followed by introduction of techniques to alleviate these issues.

The following terminology shall be used frequently hereafter. Of particular note is that we make a distinction between the turbulent flux *parameterization* and the turbulent flux *algorithm*.

- *Turbulent flux parameterization*: the equations that describe the scaling parameters, u_*, θ_*, and q_*, i.e. (8) in Section 2.2.
- *Turbulent flux algorithm or iterative method*: the numerical method used to compute a solution of the turbulent flux parameterization, e.g. Algorithm 1 in Section 2.2. Such an algorithm/method is called *convergent* if the iterates converge to a solution of the parameterization.
- *Equations underlying the turbulent flux algorithm*: the turbulent flux parameterization.
- *Existence of a solution (to the underlying equations)*: at least one solution can be determined which satisfies the equations underlying the turbulent flux algorithm.
- *Uniqueness of a solution (to the underlying equations)*: exactly one solution satisfies the equations underlying the turbulent flux algorithm.
- *Well-posed equation or parameterization*: an equation or set of equations for which there exists a unique solution.

2.1 E3SM Model

The E3SMv2 is the Earth system model developed by the U.S. Department of Energy (Golaz et al., 2019) that includes components for the atmosphere, ocean, sea ice, ice sheets, and rivers. In this study, we run E3SMv2 for 10 model years with active atmosphere, land, and rivers. External forcing conditions including sea surface temperatures and sea ice fraction, aerosol emissions, etc. are specified using the climatological mean of 2005–2014 with repeating annual cycles. We refer to such simulations as F2010 following E3SM's naming convention for model configurations. The atmosphere model, the E3SMv2 Atmosphere Model (EAMv2), has undergone a number of changes and tuning from v1 to v2 (Xie et al., 2018; Ma et al., 2022).

We produce two different F2010 simulations: CTRL, which uses the default ocean-atmosphere flux algorithm (see Section 2.2, Algorithm 1), and SENS, which uses the algorithm developed in this work that ensures that the parameterization is well-posed (see Section 3.5, Algorithm 3). In these simulations, we employ the CondiDiag tool (Wan et al., 2022) to obtain daily instantaneous output of near-surface and surface quantities to use as input for offline turbulent flux calculations and analysis.

2.2 Ocean-atmosphere turbulent flux algorithm

The focus of this work is on the default ocean-atmosphere exchange algorithm (W. Large & Pond, 1982) in E3SM inherited from the Community Earth System Model (CESM) (Hurrell et al., 2013). An initial estimate of the scaling parameters is made assuming neutral stability:

$$\begin{cases} u_* = C_{DN}(U) \cdot U \\ u_{10N} = U \\ \theta_* = C_{HN}(\Delta\theta) \cdot \Delta\theta \\ q_* = C_{EN} \cdot \Delta q, \end{cases} \tag{5}$$

where $\Delta\theta = \theta_a - \theta_s$, $\Delta q = q_a - q_s$, and C_{DN}, C_{HN}, and C_{EN} are neutral exchange coefficients defined as follows. The neutral momentum exchange, or drag, coefficient C_{DN} is determined from the 10-m neutral wind speed u_{10N} using an empirical expression derived in W. G. Large & Pond (1981):

$$C_{DN}(u_{10N}) = \frac{0.0027}{u_{10N}} + 0.000142 + 0.0000764 u_{10N}.$$

The remaining neutral exchange coefficients are defined as

$$C_{HN}(\zeta) = \begin{cases} 0.0327, & \text{if } \zeta < 0 \\ 0.018, & \text{if } \zeta > 0, \end{cases} \qquad C_{EN} = 0.0346.$$

Two additional iterations are made accounting for the effects of stability and to shift the exchange coefficients up to measurement height. Therefore, the non-neutral exchange coefficients are derived from the neutral exchange coefficients:

$$\begin{aligned} C_D(u_{10N}, \zeta(u_*, \theta_*, q_*)) &= \frac{\sqrt{C_{DN}(u_{10N})}}{1 + \frac{\sqrt{C_{DN}(u_{10N})}}{k}[\ln(\frac{z}{10}) - \psi_m(\zeta(u_*, \theta_*, q_*))} \\ C_H(\zeta(u_*, \theta_*, q_*)) &= \frac{C_{HN}(\zeta(u_*, \theta_*, q_*))}{1 + \frac{C_{HN}(\zeta(u_*, \theta_*, q_*))}{k}[\ln(\frac{z}{10}) - \psi_h(\zeta(u_*, \theta_*, q_*))]} \\ C_E(\zeta(u_*, \theta_*, q_*)) &= \frac{C_{EN}}{1 + \frac{C_{EN}}{k}[\ln(\frac{z}{10}) - \psi_q(\zeta(u_*, \theta_*, q_*))]}, \end{aligned} \tag{6}$$

where ψ_m, ψ_h, and ψ_q are the stability functions for momentum, heat, and humidity, respectively. The stability functions are defined piecewise for stable and unstable conditions as

$$\psi_m(\zeta) = \begin{cases} \ln\left([1+\chi(\zeta)(2+\chi(\zeta))](\frac{1+\chi(\zeta)^2}{8})\right) - 2\tan^{-1}\chi(\zeta) + \frac{\pi}{2}, & \zeta \leqslant 0 \\ -5\zeta, & \zeta > 0 \end{cases}$$

$$\psi_h(\zeta) = \psi_q(\zeta) = \begin{cases} \ln(\frac{1+\chi^2(\zeta)}{2}), & \zeta \leqslant 0 \\ -5\zeta, & \zeta > 0, \end{cases}$$

where $\chi(\zeta) = (1-16\zeta)^{1/4}$.

The default turbulent flux parameterization in E3SM applies a limiter to prevent the magnitude of ζ from growing too large. The limited stability parameter, which we denote by $\tilde{\zeta}$, is defined by

$$\tilde{\zeta}(u_*, \theta_*, q_*; \zeta_{\max}) = \min\{|\zeta(u_*, \theta_*, q_*)|, \zeta_{\max}\} \cdot \operatorname{sgn}(\zeta(u_*, \theta_*, q_*)). \tag{7}$$

We refer to the parameter $\zeta_{\max} > 0$ as the *limiting parameter*. Its value is set to 10 in the default turbulent flux algorithm. A detailed analysis of the stability limiter and its relationship with uniqueness of solutions of (8) is provided in Section 3.5.1.

Algorithm 1 summarizes the default ocean-atmosphere turbulent flux algorithm in E3SM. Of particular note is that the neutral 10-m wind speed is updated first, followed by simultaneous updates to the scaling parameters. Additionally, with numerical methods such as the one described in Algorithm 1, a common practice for evaluating when to stop performing more iterations is to verify whether the relative residual $|y_{n+1} - y_n|/|y_n|$, where $y \in \{u_*, u_{10N}, \theta_*, q_*\}$, is within a desired tolerance or the number of iterations has reached a specified maximum. In contrast, the default E3SM ocean-atmosphere turbulent flux algorithm described in Algorithm 1 always performs two iterations. No checks of the residuals are performed to ascertain whether convergent behavior is observed and the residual is acceptably small.

The system of equations iteratively solved by Algorithm 1, which we call the turbulent flux parameterization, can be summarized as

$$\begin{cases} u_* = C_D(u_{10N}, \zeta(u_*, \theta_*, q_*)) \cdot U \\ u_{10N} = \dfrac{C_D(u_{10N}, \zeta(u_*, \theta_*, q_*))}{\sqrt{C_{DN}(u_{10N})}} \cdot U \\ \theta_* = C_H(\zeta(u_*, \theta_*, q_*)) \cdot \Delta\theta \\ q_* = C_E(\zeta(u_*, \theta_*, q_*)) \cdot \Delta q. \end{cases} \tag{8}$$

Algorithm 1 Default atmosphere-ocean iteration in E3SM.

Input: Bulk variables U, $\Delta\theta$, and Δq and limiting parameter $\zeta_{\max}$.

Output: Approximation $(u_*)_n$, $(u_{10N})_n$, $(\theta_*)_n$, and $(q_*)_n$ to the turbulent flux parameterization (8).

1: **procedure** DefaultIteration(U, $\Delta\theta$, Δq, $\zeta_{\max}$)

2: Compute the initial estimate based on neutral conditions

$$
\begin{aligned}
(u_{10N})_0 &= U \\
(u_*)_0 &= \sqrt{C_{DN}(U)} \cdot U \\
(\theta_*)_0 &= C_{HN}(\Delta\theta) \cdot \Delta\theta \\
(q_*)_0 &= C_{EN} \cdot \Delta q
\end{aligned}
$$

3: Compute limited stability parameter $\tilde{\zeta}_0 = \tilde{\zeta}((u_*)_0, (\theta_*)_0, (q_*)_0; \zeta_{\max})$ according to (7).

4: **for** n = 1, 2 **do**

5: Update 10-m neutral wind speed:

$$(u_{10N})_n = \frac{C_D((u_{10N})_{n-1}, \tilde{\zeta}_{n-1})}{\sqrt{C_{DN}((u_{10N})_{n-1})}} \cdot U$$

6: Apply updated 10-m neutral wind speed to simultaneously update scaling parameters:

$$\begin{pmatrix} (u_*)_n \\ (\theta_*)_n \\ (q_*)_n \end{pmatrix} = \begin{pmatrix} C_D((u_{10N})_n, \tilde{\zeta}_{n-1}) \cdot U \\ C_H(\tilde{\zeta}_{n-1}) \cdot \Delta\theta \\ C_E(\tilde{\zeta}_{n-1}) \cdot \Delta q \end{pmatrix}.$$

7: Update stability parameter $\tilde{\zeta}_n = \tilde{\zeta}((u_*)_n, (\theta_*)_n, (q_*)_n; \zeta_{\max})$.

8: **end for**

9: **return** $(u_*)_n, (\theta_*)_n, (q_*)_n$.

10: **end procedure**

We note here that (8) shifts the 10-m neutral transfer coefficients to the height and stability of the atmospheric state variables (W. B. Large, 2006). The system (8) may be written in the form

$$\mathbf{x} = \mathbf{f}(\mathbf{x}) \tag{9}$$

where $\mathbf{x} = (u_*, u_{10N}, \theta_*, q_*)^T$ and $\mathbf{f}$ is the vector-valued function on the right-hand side of (8). Solutions of (9) are known as fixed points of the function $\mathbf{f}$. At such points, the scaling parameters u_*, θ_*, q_*, and neutral 10-m wind speed u_{10N} are unchanged under the transformation $\mathbf{f}$. No closed form solution of (8) in terms of elementary functions is currently known. Instead, an approximate solution is obtained from an iterative procedure such as the one described in Algorithm 1.

The iterative procedure in Algorithm 1 more generally falls under the framework of nonlinear Gauss-Seidel iterations (Ortega & Rockoff, 1966) which produce a sequence of iterates $\{\mathbf{x}_n\}$ that satisfy

$$\mathbf{g}(\mathbf{x}_{n+1}, \mathbf{x}_n) = \mathbf{0} \tag{10}$$

for a given iteration function, $\mathbf{g}$, with the initial guess, $\mathbf{x}_0$, given by neutral 10-m conditions as in (5). Given two generic vectors, $\mathbf{r}, \mathbf{s} \in \mathbb{R}^4$, the function, $\mathbf{g}$, that corresponds to the iteration in Algorithm 1 takes the form

$$\mathbf{g}(\mathbf{r}, \mathbf{s}) = \begin{pmatrix} r_1 - C_D(r_2, \zeta(s_1, s_3, s_4)) \cdot U \\ r_2 - \frac{C_D(s_2, \zeta(s_1, s_3, s_4))}{\sqrt{C_{DN}(s_2)}} \cdot U \\ r_3 - C_H(\zeta(s_1, s_3, s_4)) \cdot \Delta\theta \\ r_4 - C_E(\zeta(s_1, s_3, s_4)) \cdot \Delta q \end{pmatrix}. \tag{11}$$

As $n \to \infty$, a desirable property of iterations such as (10) is that the iterates $\mathbf{x}_n$ converge to the true solution of (9), $\mathbf{x}_*$. We shall discuss shortly in Section 3.1 the conditions under which such a convergence property can be expected.

Lastly, we note that taking $\mathbf{g}(\mathbf{x}_{n+1}, \mathbf{x}_n) := \mathbf{x}_{n+1} - \alpha\mathbf{f}(\mathbf{x}_n) - (1-\alpha)\mathbf{x}_n$ for $0 < \alpha \leqslant 1$ yields the damped fixed point iteration

$$\mathbf{x}_{n+1} = \alpha\mathbf{f}(\mathbf{x}_n) + (1-\alpha)\mathbf{x}_n. \tag{12}$$

This iteration (12) and its theory are closely related to the nonlinear Gauss-Seidel iteration (10). Given the convergence theory for the fixed point iteration is more straightforward than for the nonlinear Gauss-Seidel iteration, the related theory for the fixed point iteration is presented in Section 3.1 to provide the reader with an understanding of the relevant conditions required for (8) to have a solution and for the iteration (10) to converge.

3 Analysis

The well-posedness of a system of equations such as (8) plays a large part in determining the convergence (or lack thereof) of numerical methods, such as the one described in Algorithm 1, that attempt to approximate solutions to these equations. For example, a system with multiple solutions can result in numerical methods oscillating between those solutions, and a system with no solutions will effectively ensure no numerical method will converge. Thus, it is important that well-posedness of turbulent flux parameterizations be analyzed prior to the application of any numerical methods. To the best of our knowledge, this analysis has not yet been carried out for the turbulent flux parameterization (8).

Our analysis consists of two components. The first part, described in Section 3.1, answers the question of whether there always exists a solution to the turbulent flux parameterization (8). The second part, described in Section 3.5, answers the question of whether a solution to the turbulent flux parameterization is unique.

3.1 Existence of the scaling parameters

It will be useful in the proceeding analysis to view the turbulent flux parameterization in the form (9). The existence of a solution to (9) is typically proven by appealing to established results on contraction mappings. The function $\mathbf{f}$ in (9) is a contraction mapping if it maps any two distinct points to points that are closer together. Formally, this means that there exists $0 < \lambda < 1$ such that

$$||\mathbf{f}(\mathbf{x}) - \mathbf{f}(\mathbf{y})|| \leqslant \lambda ||\mathbf{x} - \mathbf{y}|| \tag{13}$$

for all $\mathbf{x}$ and $\mathbf{y}$. Both existence and uniqueness of a fixed point of $\mathbf{f}$ are only guaranteed when $\mathbf{f}$ is a contraction mapping within some region around the initial iterate $\mathbf{x}_0$ (Isaacson & Keller, 1994). This result is summarized in Theorem 1. In the case when $\mathbf{f}$ is not a contraction mapping, existence and uniqueness of a solution to (8) are generally not guaranteed.

Theorem 1 ((Isaacson & Keller, 1994, §3.3 Theorem 1))**.** *Let $\mathbf{x}_0$ denote the initial iterate to (12) and suppose $\mathbf{f}$ is a contraction mapping with constant $\lambda \in (0, 1)$ for all $\mathbf{x}, \mathbf{y}$ satisfying $||\mathbf{x} - \mathbf{x}_0|| < \rho$, $||\mathbf{y} - \mathbf{x}_0|| < \rho$. Suppose also that the initial iterate $\mathbf{x}_0$ satisfies*

$$||\mathbf{f}(\mathbf{x}_0) - \mathbf{x}_0|| < (1 - \lambda)\rho. \tag{14}$$

Then for $\alpha = 1$, the iteration (12) has the following properties.

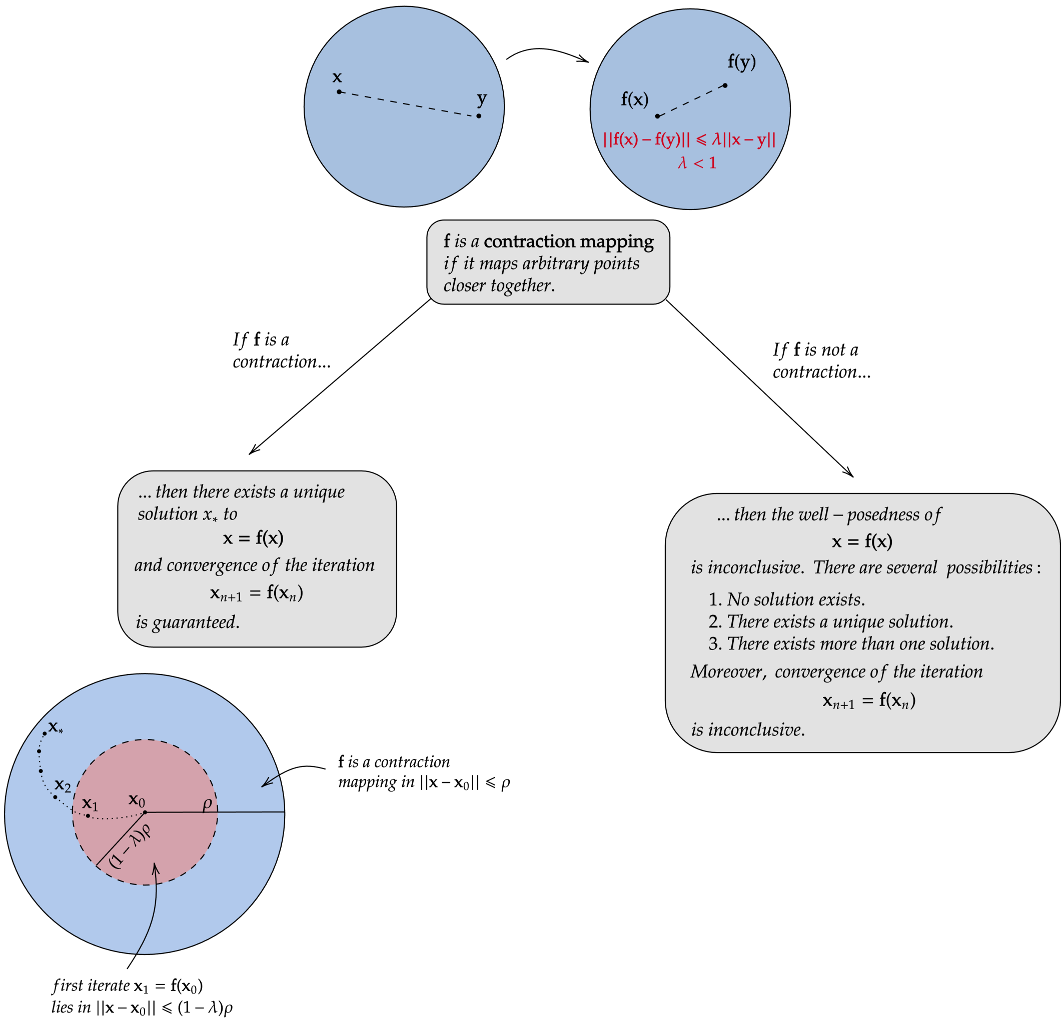

Figure 1: Visualization of (i) contraction mapping and (ii) Theorem 1. If $\mathbf{f}$ is a locally contractive mapping and the initial iterate $\mathbf{x}_1 = \mathbf{f}(\mathbf{x}_0)$ is within the $(1-\lambda)r$ ball centered at $\mathbf{x}_0$, then the sequence $\mathbf{x}_{n+1} = \mathbf{f}(\mathbf{x}_n)$ is guaranteed to converge to a solution $\mathbf{x}_*$.

1. *All iterates* $\mathbf{x}_n$ *satisfy*

$$||\mathbf{x}_n - \mathbf{x}_0|| \leqslant \rho.$$

2. *The iterates converge to a vector* $\mathbf{x}_*$ *which is a solution of* (9)*:*

$$\lim_{n\to\infty} \mathbf{x}_n = \mathbf{x}_*, \textit{ where } \mathbf{x}_* = \mathbf{f}(\mathbf{x}_*).$$

3. *The solution* $\mathbf{x}_*$ *is the only solution of* (9) *in* $||\mathbf{x} - \mathbf{x}_0|| \leqslant \rho$.

In general, Theorem 1 provides sufficient but not necessary conditions for local existence and uniqueness of the fixed point, i.e., a violation of condition (13) or (14) does not

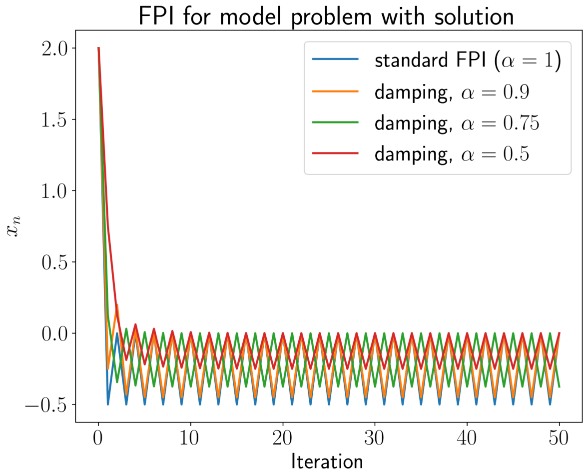

Figure 2: Standard fixed point iteration with various values of the damping parameter α for the function h in (15) which has no fixed points. The iteration oscillates regardless of choice of method because there is no solution satisfying $x = h(x)$.

necessarily mean that a unique fixed point does not exist. Nevertheless, since the function $\mathbf{f}$ corresponding to the turbulent flux parameterization (8) contains a jump discontinuity due to the discontinuous definition of the exchange coefficient C_{HN}, we note that $\mathbf{f}$ can never satisfy the contraction property (13). Moreover, we shall demonstrate that this discontinuity leads in some scenarios to the non-existence of a solution of (8) which manifests in the iteration (12) as an oscillating iterate $\mathbf{x}_n$.

Before illustrating the impact of discontinuities in the turbulent flux parameterization (8), we first consider a simpler problem which is emblematic of issues encountered in (8). Consider computing the fixed points of the simple function

$$h(x) = \begin{cases} x + 1/2, & x \leqslant 0 \\ -1/2, & x > 0. \end{cases} \tag{15}$$

The function h has no fixed points, i.e. $x = g(x)$ has no solutions. Moreover, applying (12) with various damping parameters for 100 iterations, we observe that x_n oscillates infinitely between $-1/2$ and $1/4$. Figure 2 shows a history of the iterate x_n as well as a graph of h. The oscillations observed in this simple example are indicative of the iteration behavior that occurs under certain conditions for the turbulent flux parameterization (8).

We next turn our attention to the impact of discontinuities in the turbulent flux parameterization (8) on convergence of the default E3SM iteration described in Algorithm 1.

The third equation of (8) may be written in expanded form as

$$\theta_* = \frac{C_{HN}(\zeta)}{1 + \frac{C_{HN}(\zeta)}{k}(\ln(z/10) - \psi_h(\zeta))}\Delta\theta =: f_3(\zeta). \tag{16}$$

Figure 3 shows graphs of C_{HN} and f_3 as functions of the stability parameter ζ. In general, f_3 always contains a discontinuity due to the discontinuous behavior of C_{HN}. However, issues only arise when the meteorological variables are such that the solution of (8) would lie along the discontinuity of f_3. One such example arises for the meteorological conditions given by

$$U = 0.35 \text{ m/s}, \quad z = 13.36 \text{ m}, \quad \theta_s = 299.29 \text{ K}, \quad \theta_a = 299.83 \text{ K}, \quad q_a = 18.85 \text{ g/kg}. \tag{17}$$

We apply Algorithm 1 to this example for 100 iterations. For brevity, we only show results for the iterate θ_n and its residual $|\theta_{n+1} - \theta_n|/|\theta_n|$ (Figure 4) and note that while oscillations are present in all solution variables, they are most strongly observed in θ_* that is derived from f_3. The relative residual error in θ_* for this example is approximately 50% and indicates that the computed scaling parameters do not satisfy the underlying equations that comprise the turbulent flux parameterization (8).

While the oscillatory results in Figure 4 do not necessarily mean there is no solution to (8) for the scenario described by (17), the simple example shown here suggests that the oscillations in the iterate $\mathbf{x}_n$ are possibly caused by the discontinuity in C_{HN}. Indeed, we shall demonstrate in Section 3.2 that a small modification to C_{HN} to remove the discontinuity at $\zeta = 0$ eliminates the oscillations entirely and allows the iteration to converge to a solution.

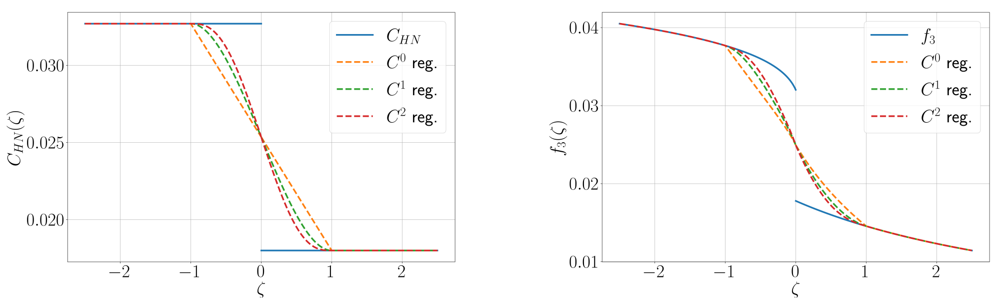

Figure 3: (left) Neutral exchange coefficient of heat and its regularizations. (right) Iteration function f_3 and its regularizations.

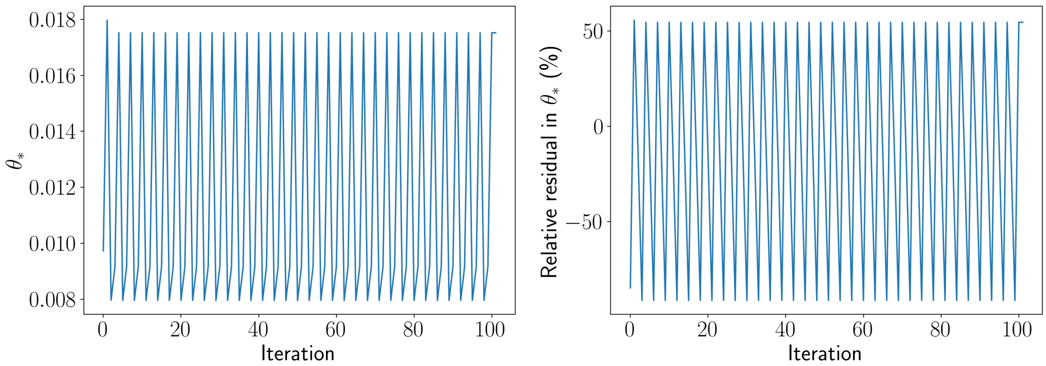

Figure 4: The iterate θ_n and the relative residual in $|\theta_{n+1} - \theta_n|/|\theta_n|$ when approximating the solution of the turbulent flux parameterization (8) with conditions described by (17). The iterates are described by Algorithm 1 with the exception that 100 iterations are performed rather than 2.

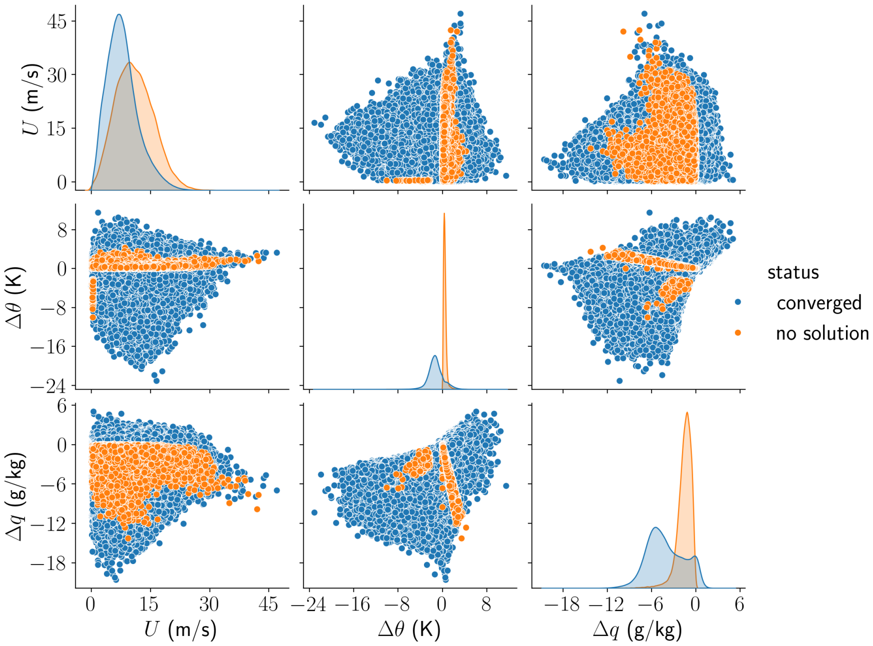

Figure 5: A corner plot showing the marginal probability distributions and pairwise scatter plots of the variables U, $\Delta\theta$, and Δq for both atmospheric conditions that have no solution and those whose iteration converges to a solution. The U, $\Delta\theta$, and Δq samples used here are 10 years of daily instantaneous output from the CTRL simulation. The classification ("converged" versus "no solution") was done in offline calculations using Algorithm 1 and 100 iterations.

It is difficult to definitively determine which sets of meteorological variables result in Algorithm 1 exhibiting oscillatory behavior. Nevertheless, to provide some insight into the conditions which generate the scenario observed in Figure 4, we consider ten years of data from the F2010 simulation CTRL, utilizing the CondiDiag tool (Wan et al., 2022) to write out daily instantaneous values for the state variables. Using these daily values, we perform 100 iterations of Algorithm 1, and each data point is classified as either (i) having no solution if it exhibits oscillatory behavior or (ii) having converged if the relative residuals for each solution field are less than 10^{-10}. The marginal probability distributions for U, $\Delta\theta$, and Δq are provided in the main diagonal of Figure 5 for both data points with no solution and data points that have converged to a solution. Off-diagonal entries show the pairwise scatter plots of U, $\Delta\theta$, and Δq for each class of data. The main condition in which there is usually a lack of convergence in the solution of (8) is approximately 0 K $< \Delta\theta <$ 0.7 K.

With conditions identified in which there might be a lack of convergence in (8), we explore how often the model exhibits these conditions. Figure 6 shows the percentage of days in which 0 K $< \Delta\theta$ (between surface and air) $<$ 0.7 K for the months of December, January, and February (hereinafter DJF) as well as June, July, and August (hereinafter JJA). In DJF, the most frequent occurrences of these conditions are in the Southern Ocean along the ice edge. Higher frequencies are also found in the mid-latitude storm tracks over the North Atlantic and Pacific Oceans. In JJA, the most frequent occurrences are over the North Atlantic and Pacific just south of the ice edge, as well as over the Arabian Sea.

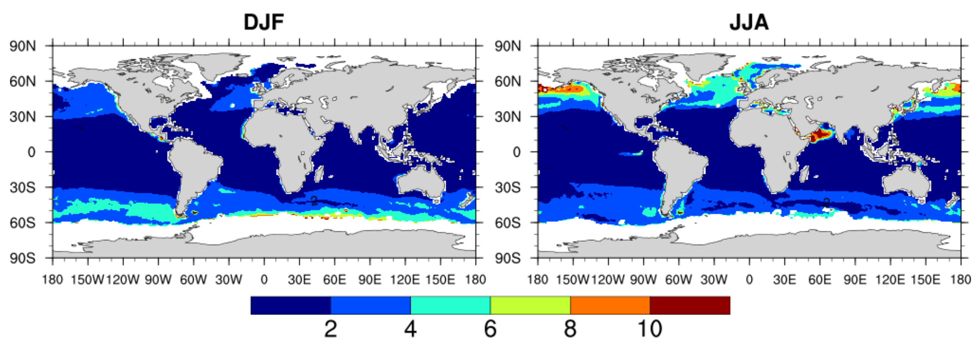

Figure 6: Percentage of days for which the daily instantaneous output of $\Delta\theta$ in DJF (left) or JJA (right) falls in the range of 0 K to 0.7 K in 10 years of the CTRL simulation. Gray shading indicates land, and white areas are sea ice.

3.2 Regularization of heat exchange coefficient

To enforce continuity of the heat exchange coefficient C_{HN}, we propose a simple C^k regularization which replaces the jump discontinuity with a polynomial function $p^{(k)}_{\varepsilon_{\text{reg}}}$ allowing the regularized coefficient, $\tilde{C}^{(k)}_{HN\varepsilon_{\text{reg}}}$, to have k continuous derivatives:

$$\tilde{C}^{(k)}_{HN,\varepsilon_{\text{reg}}}(\zeta) := \begin{cases} 0.0327, & \zeta \leqslant -\varepsilon_{\text{reg}} \\ p^{(k)}_{\varepsilon_{\text{reg}}}(\zeta), & -\varepsilon_{\text{reg}} < \zeta \leqslant \varepsilon_{\text{reg}} \\ 0.018, & \zeta > \varepsilon_{\text{reg}} \end{cases}, \quad p^{(k)}_{\varepsilon_{\text{reg}}}(\zeta) := \sum_{j=0}^{2k+1} a_j \zeta^j, \quad \varepsilon_{\text{reg}} > 0.$$

The coefficients, a_j, are obtained by enforcing the continuity conditions

$$p^{(k)}_{\varepsilon_{\text{reg}}}(-\varepsilon_{\text{reg}}) = 0.0327, \quad p^{(k)}_{\varepsilon_{\text{reg}}}(\varepsilon_{\text{reg}}) = 0.018, \quad \left.\frac{d^j p_{k,\varepsilon_{\text{reg}}}}{d\zeta^j}\right|_{\zeta=\pm\varepsilon_{\text{reg}}} = 0, \quad 1 \leqslant j \leqslant k,$$

which amounts to solving a system of $2k+2$ linear equations. For completeness, we state the C^0 and C^1 polynomials below:

$$p^{(0)}_{\varepsilon_{\text{reg}}}(\zeta) = 0.02535 - \frac{0.00735}{\varepsilon_{\text{reg}}}\zeta$$
$$p^{(1)}_{\varepsilon_{\text{reg}}}(\zeta) = 0.02535 - \frac{0.011025}{\varepsilon_{\text{reg}}}\zeta + \frac{0.003675}{\varepsilon^3_{\text{reg}}}\zeta^3.$$

An example of the regularization for $\varepsilon_{\text{reg}} = 1$ is shown in Figure 3. With the regularized coefficient $\tilde{C}^{(k)}_{HN,\varepsilon_{\text{reg}}}$, we may define the regularized turbulent exchange coefficient $\tilde{C}^{(k)}_{H,\varepsilon_{\text{reg}}}$ by

$$\tilde{C}^{(k)}_{H,\varepsilon_{\text{reg}}}(\zeta(u_*,\theta_*,q_*)) := \frac{\tilde{C}^{(k)}_{HN,\varepsilon_{\text{reg}}}(\zeta(u_*,\theta_*,q_*))}{1 + \frac{\tilde{C}^{(k)}_{HN,\varepsilon_{\text{reg}}}(\zeta(u_*,\theta_*,q_*))}{k}[\ln(\frac{z}{10}) - \psi_h(\zeta(u_*,\theta_*,q_*))]} \tag{18}$$

to replace the discontinuous coefficient C_H in (8). The regularized turbulent flux parameterization based on the Large and Pond parameterization (8) and the regularization (18) is given by

$$\begin{cases} u_* = C_D(u_{10N}, \zeta(u_*,\theta_*,q_*)) \cdot U \\ u_{10N} = \dfrac{C_D(u_{10N}, \zeta(u_*,\theta_*,q_*))}{\sqrt{C_{DN}(u_{10N})}} \cdot U \\ \theta_* = \tilde{C}^{(k)}_{H,\varepsilon_{\text{reg}}}(\zeta(u_*,\theta_*,q_*)) \cdot \Delta\theta \\ q_* = C_E(\zeta(u_*,\theta_*,q_*)) \cdot \Delta q. \end{cases} \tag{19}$$

The regularization parameter ε_{reg} determines how much of the original exchange coefficient C_{HN} is replaced by the polynomial $p_{k,\varepsilon_{\text{reg}}}$. In principle, any positive value of ε_{reg} ensures that the range of $\mathbf{f}$ is a connected region in $\mathbb{R}^4$ and thus, the oscillatory behavior in Algorithm 1 should be avoided. However, in practice, smaller values of ε_{reg} will preserve more of the original exchange coefficient but may not alleviate the problem of oscillating

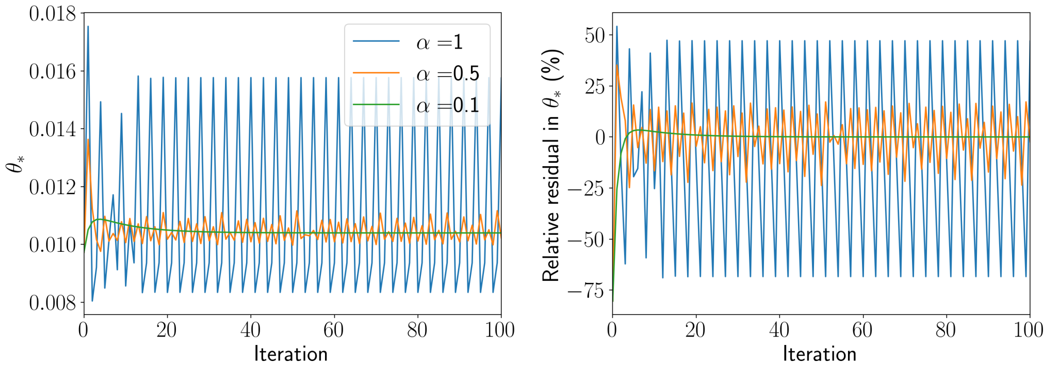

Figure 7: The iterate θ_n and the relative residual in $|\theta_{n+1}-\theta_n|/|\theta_n|$ when approximating the solution of the regularized turbulent flux parameterization (19) with conditions described by (17). The value of the regularization parameter is $\varepsilon_{\text{reg}} = 0.1$. The iterates are described by the nonlinear Gauss-Seidel iteration (20) with damping parameters chosen from $\alpha \in \{1, 0.5, 0.1\}$.

iterations due to the sharp gradient associated with small ε_{reg}. On the other hand, larger values of ε_{reg} make it easier for numerical methods to converge to a solution of (19) but modify more of the original exchange coefficient. Thus, care must be taken in choosing ε_{reg} so that the key features of the original exchange coefficient are preserved while also not making it onerously difficult for iterative methods to converge to a solution.

3.3 Damped fixed point iteration for the regularized system

Convergence of the iteration applied to the regularized parameterization (19) requires the use of damping (cf. equation (12)). To see this, we apply a variant of the default iteration described in Algorithm 1 which introduces a damping parameter $\alpha > 0$ to the regularized turbulent flux parameterization (19) with $\varepsilon_{\text{reg}} = 0.1$ for the example described by (22). This iteration may be described by the nonlinear system $\tilde{\mathbf{g}}(\mathbf{x}_{n+1}, \mathbf{x}_n) = \mathbf{0}$, where $\tilde{\mathbf{g}}$ is the function

$$\tilde{\mathbf{g}}(\mathbf{r}, \mathbf{s}) = \begin{pmatrix} r_1 - \alpha C_D(r_2, \zeta(s_1, s_3, s_4)) \cdot U - (1-\alpha)s_1 \\ r_2 - \alpha \frac{C_D(s_2, \zeta(s_1, s_3, s_4))}{\sqrt{C_{DN}(t_2)}} \cdot U - (1-\alpha)s_2 \\ r_3 - \alpha \tilde{C}^{(k)}_{H,\varepsilon_{\text{reg}}}(\zeta(s_1, s_3, s_4)) \cdot \Delta\theta - (1-\alpha)s_3 \\ r_4 - \alpha C_E(\zeta(s_1, s_3, s_4)) \cdot \Delta q - (1-\alpha)s_4 \end{pmatrix}. \tag{20}$$

We apply the iteration described by (20) with 100 iterations and vary the damping parameter from $\alpha \in \{1, 0.5, 0.1\}$ (Figure 7). It is clear that the damped iteration (20) converges to the solution of the turbulent flux parameterization (19) so long as the damping parameter is chosen carefully. In particular, if α is too large relative to ε_{reg}, the oscillations are still present at varying levels depending on the value of α chosen.

3.4 Stopping criterion

Before presenting the full algorithm for approximating the regularized turbulent flux parameterization (19), we discuss convergence criteria for terminating the iterative process. The default E3SM iteration in Algorithm 1 takes two iterations before terminating and returning the second iterate as the approximation to the scaling parameters. In practice, such iterations are typically terminated by utilizing a convergence test and terminating the iteration if the convergence test is passed or a maximum number of iterations is taken. Given $(u_*, u_{10N}, \theta_*, q_*)$, we define the residual

$$\mathcal{R}(u_*, u_{10N}, \theta_*, q_*) := \sqrt{\sum_{i=1}^{4} |r_i(u_*, u_{10N}, \theta_*, q_*)|^2}, \tag{21}$$

where

$$\begin{aligned}
r_1(u_*, u_{10N}, \theta_*, q_*) &= \frac{u_* - C_D(u_{10N}, \zeta(u_*, \theta_*, q_*)) \cdot U}{u_*} \\
r_2(u_*, u_{10N}, \theta_*, q_*) &= \frac{u_{10N} - C_D(u_{10N}, \zeta(u_*, \theta_*, q_*))/\sqrt{C_{DN}(u_{10N})} \cdot U}{u_{10N}} \\
r_3(u_*, u_{10N}, \theta_*, q_*) &= \frac{\theta_* - \tilde{C}^{(0)}_{H,\varepsilon_{\text{reg}}}(\zeta(u_*, \theta_*, q_*)) \cdot \Delta\theta}{\theta_*} \\
r_4(u_*, u_{10N}, \theta_*, q_*) &= \frac{q_* - C_E(\zeta(u_*, \theta_*, q_*)) \cdot \Delta q}{q_*}
\end{aligned}$$

are the component relative residuals for each scaling parameter and may be viewed as the relative change from the current iteration to the next iteration. We note here that (21) is simply the ℓ^2 norm of the component residuals.

Algorithm 2 Regularized atmosphere-ocean iteration.

Input: Bulk variables U, $\Delta\theta$, and Δq; limiting parameter $\zeta_{\max}$; damping parameter $\alpha \in (0, 1]$; tolerance `tol`; maximum iterations `maxiter`.

Output: Approximation $(u_*)_n$, $(u_{10N})_n$, $(\theta_*)_n$, and $(q_*)_n$ to the turbulent flux parameterization (19).

procedure RegularizedIteration(U, $\Delta\theta$, Δq, $\zeta_{\max}$, α, `tol`, `maxiter`)

  Set $n = 0$.

  Compute the initial estimate based on neutral conditions

$$\begin{aligned}(u_{10N})_n &= U \\ (u_*)_n &= C_{DN}(U) \cdot U \\ (\theta_*)_n &= \tilde{C}^{(0)}_{HN,\varepsilon_{\text{reg}}}(\Delta\theta) \cdot \Delta\theta \\ (q_*)_n &= C_{EN} \cdot \Delta q\end{aligned}$$

  Compute limited stability parameter $\tilde{\zeta}_n = \tilde{\zeta}((u_*)_n, (\theta_*)_n, (q_*)_n; \zeta_{\max})$ according to (7).

  while $\mathcal{R}((u_*)_n, (u_{10N})_n, (\theta_*)_n, (q_*)_n) >$ `tol` **do**

    Increment $n \leftarrow n + 1$.

    Update 10-m neutral wind speed using regularized coefficients:

$$(u_{10N})_n = \alpha \frac{C_D((u_{10N})_{n-1}, \tilde{\zeta}_{n-1})}{\sqrt{C_{DN}((u_{10N})_{n-1})}} \cdot U + (1 - \alpha) \cdot (u_{10N})_{n-1}.$$

    Apply updated 10-m neutral wind speed to simultaneously update scaling parameters using regularized coefficients:

$$\begin{pmatrix} (u_*)_n \\ (\theta_*)_n \\ (q_*)_n \end{pmatrix} = \alpha \begin{pmatrix} \sqrt{C_D((u_{10N})_n, \tilde{\zeta}_{n-1})} \cdot U \\ \tilde{C}^{(0)}_{H,\varepsilon_{\text{reg}}}(\tilde{\zeta}_{n-1}) \cdot \Delta\theta \\ C_E(\tilde{\zeta}_{n-1}) \cdot \Delta q \end{pmatrix} + (1 - \alpha) \begin{pmatrix} (u_*)_{n-1} \\ (\theta_*)_{n-1} \\ (q_*)_{n-1} \end{pmatrix}.$$

    Update stability parameter $\tilde{\zeta}_n = \tilde{\zeta}((u_*)_n, (\theta_*)_n, (q_*)_n.; \zeta_{\max})$.

    if $n >$ `maxiter` **then**

      Error(“Maximum iterations reached without achieving desired tolerance.”)

    end if

  end while

return $(u_*)_n, (\theta_*)_n, (q_*)_n$.

end procedure

Given the iterates $(u_*)_n$, $(u_{10N})_n$, $(\theta_*)_n$, and $(q_*)_n$, the convergence test is to check whether $\mathcal{R}((u_*)_n, (u_{10N})_n, (\theta_*)_n, (q_*)_n) < \texttt{tol}$ for a user-prescribed tolerance $\texttt{tol} > 0$. The full algorithm for approximating the scaling parameters described by the turbulent flux parameterization (19) is given in Algorithm 2. As is standard with such iterative methods, the iteration is terminated and an error message returned to the user if the number of iterations exceeds a specified `maxiter` without achieving the desired tolerance.

Finally, we briefly comment on the efficiency of the proposed Algorithm 2 compared to the E3SM default Algorithm 1. One should not generally expect to obtain a high level of accuracy in the scaling parameters (and hence, the surface fluxes as well) using the default two iterations in Algorithm 1. On the one hand, practitioners of E3SM and other global models might argue that the level of accuracy achieved with two iterations is on par with the low level of accuracy obtained in other components of E3SM, for instance, first-order time integration and coupling methods (Wan et al., 2021, 2015). On the other hand, the recent exploration of higher order time integration techniques to resolve atmospheric dynamics (Vogl et al., 2019; Gardner et al., 2018) in conjunction with improvements to physics parameterizations and their coupling (Wan et al., 2024; Zhang et al., 2023) in Earth system models means that the relatively large approximation errors obtained by Algorithm 1 may not be sufficient in future updates to E3SM.

As one might expect, Algorithm 2 is usually (depending on the value of `tol`) more computationally expensive than the default E3SM algorithm. However, we note that Algorithm 1 comprises a relatively small portion of total computation time in E3SM. Increasing the number of iterations performed is not expected to substantially increase the total computation time. Nevertheless, techniques for accelerating convergence of Algorithm 2 are readily available. For example, Anderson acceleration (Anderson, 1965) updates the iteration by computing a linear combination of m previous iterates and, in many cases, converges faster than the standard fixed point and Gauss-Seidel iterations. Efficient implementations are available to Fortran codes via software libraries such as SUNDIALS (Hindmarsh et al., 2005). To demonstrate the potential benefits of Anderson acceleration, we compute the surface fluxes in an offline setup for a set of data consisting of meteorological conditions from the CTRL simulation every five days over the course of a full year using CondiDiag. Computation of the surface fluxes is done using both (i) Anderson acceleration from SUNDIALS with $m = 1$ which computes the update $\mathbf{x}_{n+1}$ using the previous iterates $\mathbf{x}_n$ and $\mathbf{x}_{n-1}$, and (ii) the standard fixed point iteration (12) which has the same computational cost as the

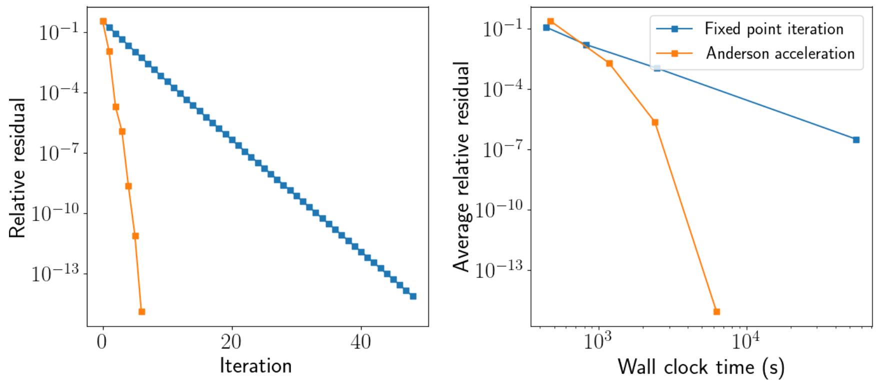

Figure 8: A demonstration of Anderson acceleration to improve convergence of scaling parameters. (left) Behavior of the relative residual $\mathcal{R}((u_*)_n, (u_{10N})_n, (\theta_*)_n, (q_*)_n)$ for approximating surface fluxes from the parameterization (19) at a single location. (right) Average residual for meteorological conditions sampled across a year of data from the CTRL simulation vs. wall clock time. Individual points correspond to fixed point and Anderson acceleration iterations with $\texttt{maxiters} = 2, 5, 10, 100$ and $\texttt{tol} = 10^{-14}$.

default E3SM iteration in Algorithm 1 (Figure 8). We observe that Anderson acceleration converges rapidly and also results in significant speed-up in wall clock time in comparison to the standard fixed point iteration. For instance, Anderson acceleration attains an average relative residual of 10^{-4} more than three times faster than the standard fixed point iteration. Thus, even if the additional computational cost of Algorithm 2 is found to be more than modest, techniques such as Anderson acceleration can substantially mitigate that cost to capitalize on the substantial improvements in solution quality over Algorithm 1.

3.5 Uniqueness of the scaling parameters

With some confidence that a solution of (19) exists, we now investigate issues of uniqueness of solutions of (19). We focus primarily on the role the stability parameter ζ plays in dictating the number of solutions of (19). No matter the value of U, $\Delta\theta$, and Δq, the stability functions $\psi_{(m,h,q)}$ are unbounded and satisfy the following property:

$$\lim_{\zeta\to\pm\infty} \psi_m(\zeta) = \lim_{\zeta\to\pm\infty} \psi_h(\zeta) = \lim_{\zeta\to\pm\infty} \psi_q(\zeta) = \mp\infty.$$

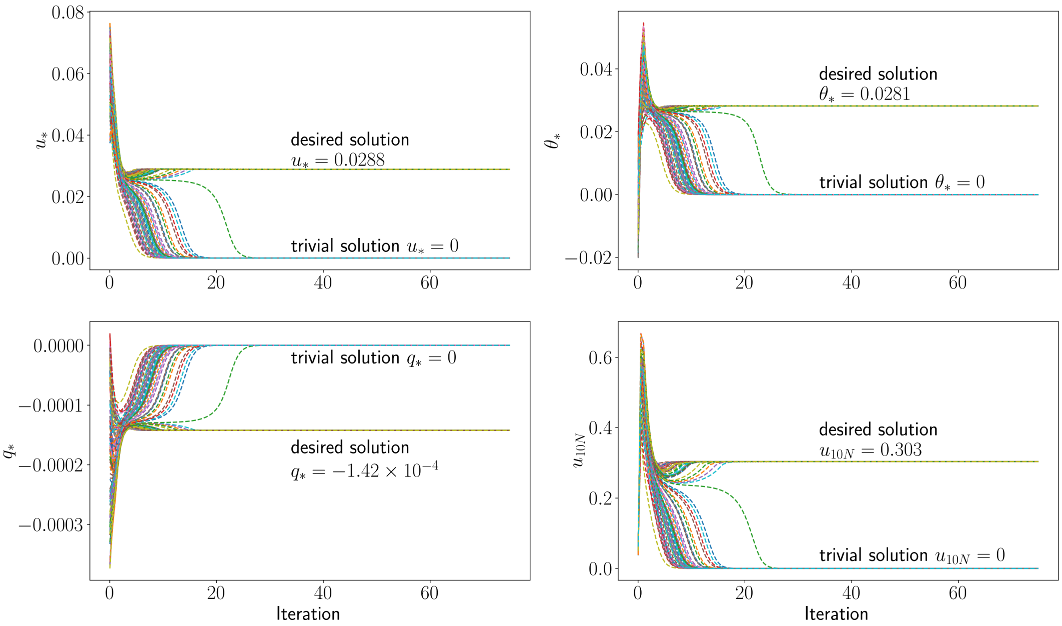

Figure 9: Progress of approximating the scaling parameters u_*, θ_*, and q_* and 10-m wind speed u_{10N} in Algorithm 2 without stability limiter. Each dashed line represents an application of Algorithm 2 with an initial guess drawn randomly from a uniform distribution. Depending on the initial guess, the iterations converge to two solutions, a trivial one at $(u_*, u_{10N}, \theta_*, q_*) = (0, 0, 0, 0)$ and a non-trivial solution $(u_*, u_{10N}, \theta_*, q_*) = (0.0288, 0.303, -0.000142, 0.0281)$.

Thus, the coefficients C_D, $\tilde{C}^{(k)}_{H,\varepsilon_{\text{reg}}}$, and C_E as defined in (6) and (18) satisfy

$$\begin{aligned}
\lim_{\zeta \to \pm\infty} \frac{\sqrt{C_{DN}(u_{10N})}}{1 + \frac{\sqrt{C_{DN}(u_{10N})}}{k}[\ln(\frac{z}{10}) - \psi_m(\zeta)]} &= 0 \\
\lim_{\zeta \to \pm\infty} \frac{\tilde{C}^{(k)}_{HN,\varepsilon_{\text{ref}}}(\zeta)}{1 + \frac{\tilde{C}^{(k)}_{HN,\varepsilon_{\text{reg}}}(\zeta)}{k}[\ln(\frac{z}{10}) - \psi_h(\zeta)]} &= 0 \\
\lim_{\zeta \to \pm\infty} \frac{C_{EN}}{1 + \frac{C_{EN}}{k}[\ln(\frac{z}{10}) - \psi_q(\zeta)]} &= 0.
\end{aligned}$$

This means that as $\zeta \to \pm\infty$, the scaling parameters converge to 0, i.e. $(u_*, \theta_*, q_*) \to (0, 0, 0)$ and $u_{10N} \to 0$.

For the specific case when

$$U = 0.1 \text{ m/s}, \quad z = 13.43 \text{ m}, \quad \theta_s = 300.04 \text{ K}, \quad \theta_a = 301.78 \text{ K}, \quad q_a = 16.87 \text{ g/kg}, \tag{22}$$

we shall demonstrate that it is indeed possible for Algorithm 2 to converge to the trivial solution $(u_*, u_{10N}, \theta_*, q_*) = (0, 0, 0, 0)$. We apply Algorithm 2 100 times without the stability limiter (i.e. $\tilde{\zeta}$ is replaced by ζ in Algorithm 1), each with a randomized initial condition, and plot the scaling parameters at each iteration of the algorithm (Figure 9). We observe two distinct solutions for this example – one at $(u_*, u_{10N}, \theta_*, q_*) = (0, 0, 0, 0)$ corresponding to the case when $\zeta \to \pm\infty$ and another non-zero solution at $(u_*, u_{10N}, \theta_*, q_*) = (0.0288, 0.303, 0.0281, -0.000142)$. Such behavior means that the turbulent flux parameterization (19) will not generally have a unique solution. Perhaps more importantly, we see that the turbulent flux parameterization has undesired solutions that Algorithm 2 will converge to.

3.5.1 Stability limiter

We now turn our attention to the stability limiter $\tilde{\zeta}$ and address its role in determining uniqueness of the surface fluxes. Recall that E3SM utilizes the stability limiter in the implementation of Algorithm 1 to prevent the magnitude of ζ from growing too large. In practice, the limiter prevents the scenario where $\zeta \to \pm\infty$. To the best of our knowledge,

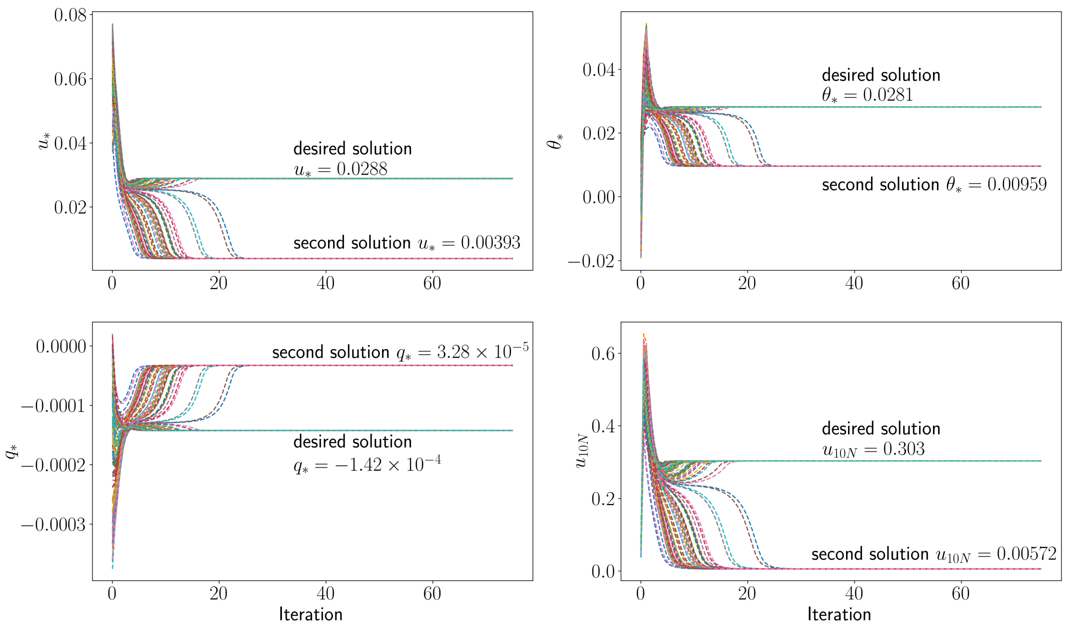

Figure 10: Progress of approximating the scaling parameters u_*, θ_*, and q_* and 10-m wind speed u_{10N} in Algorithm 2 with the limiter (7) applied with $\zeta_{max} = 10$. The physically-relevant solution remains unchanged from the case with no stability limiter (see Figure 9 while the original trivial solution at $(u_*, u_{10N}, \theta_*, q_*) = (0, 0, 0, 0)$ is shifted to $(u_*, u_{10N}, \theta_*, q_*) = (0.00393, 0.00959, -3.28 \times 10^{-5}, 0.00572)$.

no systematic analysis has been carried out to determine the effect of the limiter (7) on convergence of Algorithm 1.

One might expect that since the limiter removes the possibility that $\zeta \to \pm\infty$, the trivial solution $(u_*, u_{10N}, \theta_*, q_*) = (0, 0, 0, 0)$ should no longer exist and (8) should have a unique solution when (7) is used. However, we demonstrate that the limiter does not actually remove the second solution at $(u_*, u_{10N}, \theta_*, q*) = (0, 0, 0, 0)$ but rather shifts it away from zero. To see this, we consider the same example described by (22) but apply the limiter (7) with $\zeta_{max} = 10$ (Figure 10). We observe that the trivial solution at $(u_*, u_{10N}, \theta_*, q_*) = (0, 0, 0, 0)$ is shifted to $(u_*, u_{10N}, \theta_*, q_*) = (0.00393, 0.00959, -3.28 \times 10^{-5}, 0.00572)$ and in fact, the turbulent flux parameterization described by (19) still has two solutions even when the stability limiter is applied.

More generally, the value of the limiting parameter $\zeta_{\max}$ has a strong effect on the number of solutions of (19). When a closed form solution of a given equation is known, a systematic analysis of the effect of a model parameter on uniqueness of the solution is straightforward. For instance, one can express the solution as a function of the parameter of interest and generate a *bifurcation diagram* (Chow & Hale, 2012) which provides qualitative information on the solution of (8) for each value of the parameter. Given a closed form solution of (19) is not known, an approximate bifurcation diagram may still be generated by performing several runs of Algorithm 2 for a range of different initial guesses and observing how many distinct solutions the algorithm converges to for different values of $\zeta_{\max}$

We increase $\zeta_{\max}$ from 10^{-1} to 10^4 and consider four different meteorological conditions. Four distinct scenarios are observed as illustrated in Figure 11:

1. There is exactly one solution which does not depend on $\zeta_{\max}$ (Figure 11a).
2. There is exactly one solution which varies with $\zeta_{\max}$ until a turning point after which the solution is constant with $\zeta_{\max}$ (Figure 11b). When the solution varies with $\zeta_{\max}$,

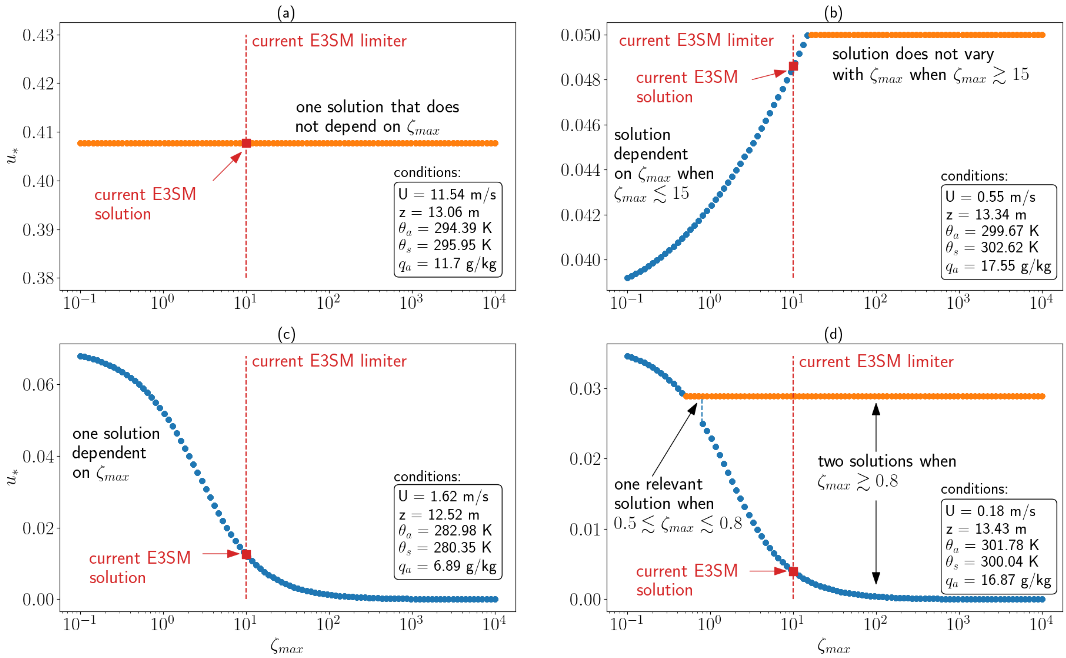

Figure 11: An overview of the possible behavior of the scaling parameters as the limiter parameter $\zeta_{\max}$ is varied. (a) There is exactly one solution which is independent of $\zeta_{\max}$. (b) There is exact one solution which varies with $\zeta_{\max}$ whenever $\zeta_{\max} \lesssim 15$ and does not vary with $\zeta_{\max}$ whenever $\zeta_{\max} \gtrsim 15$. (c) There is exactly one solution which always varies with $\zeta_{\max}$. (d) There is a bifurcation point at which the underlying equations transition from having exactly one solution to having two solutions. When two solutions exist, one of them varies with $\zeta_{\max}$ while the other does not. When one solution exists, it may vary with $\zeta_{\max}$ (e.g. for $\zeta_{\max} \lesssim 0.5$) or may be constant with $\zeta_{\max}$ (e.g. for $0.5 \lesssim \zeta_{\max} \lesssim 0.8$).

it is described implicitly by the manifold on which $|\zeta| = \zeta_{\max}$:

$$\begin{cases} u_*(\zeta_{\max}) = \dfrac{\sqrt{C_{DN}(u_{10N}(\zeta_{\max}\cdot \operatorname{sgn}(\Delta\theta)))}}{1+\frac{\sqrt{C_{DN}(u_{10N}(\zeta_{\max}\cdot\operatorname{sgn}(\Delta\theta)))}}{k}(\ln(z/10)-\psi_m(\zeta_{\max}\cdot\operatorname{sgn}(\Delta\theta)))}U \\ u_{10N}(\zeta_{\max}) = \dfrac{1}{1+\frac{\sqrt{C_{DN}(u_{10N}(\zeta_{\max}\cdot\operatorname{sgn}(\Delta\theta)))}}{k}(\ln(z/10)-\psi_m(\zeta_{\max}\cdot\operatorname{sgn}(\Delta\theta)))}U \\ \theta_*(\zeta_{\max}) = \dfrac{C_{HN}(\zeta_{\max}\cdot\operatorname{sgn}(\Delta\theta)))}{1+\frac{C_{HN}(\zeta_{\max}\cdot\operatorname{sgn}(\Delta\theta)))}{k}(\ln(z/10)-\psi_h(\zeta_{\max}\cdot\operatorname{sgn}(\Delta\theta)))}\Delta\theta \\ q_*(\zeta_{\max}) = \dfrac{C_{EN}}{1+\frac{C_{EN}}{k}(\ln(z/10)-\psi_h(\zeta_{\max}\cdot\operatorname{sgn}(\Delta\theta)))}\Delta q, \end{cases} \tag{23}$$

3. There is exactly one solution which depends on $\zeta_{\max}$ (Figure 11c). This solution is given implicitly by (23).

4. For $\zeta_{\max}$ within a certain range, there are exactly two solutions, one of which does not vary with $\zeta_{\max}$ and one of which varies with $\zeta_{\max}$ (Figure 11d). The latter is described by (23). For $\zeta_{\max}$ outside of this range, there is a unique solution which may or may not vary with $\zeta_{\max}$. The value of $\zeta_{\max}$ at which the number of possible solutions transitions from one to two is known as a *bifurcation point*.

The first scenario is ideal in the sense that the limiter has no effect on the solution. While a rigorous theory establishing precisely when this scenario occurs is beyond the mathematical techniques described in this paper, we suspect that this scenario may occur when the meteorological conditions prevent the stability parameter ζ from ever approaching the large values which induce the second solution described in Section 3.5.

The second scenario illustrates that the limiter must be chosen carefully in order to ensure that the obtained solution exhibits desirable behavior. Specifically, the obtained solution should not vary with the value of $\zeta_{\max}$. When $\zeta_{\max} \gtrsim 15$, we observe that the solution is constant with respect to $\zeta_{\max}$. It is this desired solution which a numerical method should converge to. On the other hand, if $\zeta_{\max} \lesssim 15$, we observe the undesired behavior in which the solution varies with the value of $\zeta_{\max}$. Notably, the current value of $\zeta_{\max} = 10$ in E3SM is clearly too small and would result in obtaining the undesired solution.

The third scenario in which the only solution depends on the value of $\zeta_{\max}$ suggests that there is no desired solution to the turbulent flux parameterization (19). It is impossible to ascertain which value of $\zeta_{\max}$ corresponds to a "correct" solution and may suggest that the W. Large & Pond (1982) parameterization is not valid for the range of meteorological conditions that produce this behavior. For instance, it is well known that in extremely stable conditions as $\zeta \to \infty$, the assumption of constant surface fluxes with respect to altitude is violated (Optis et al., 2016) and the Monin-Obukhov Similarity Theory that underpins the derivation of the parameterization is no longer valid.

Finally, the fourth scenario, much like the second, illustrates the importance of correctly selecting $\zeta_{\max}$ to obtain the physically relevant solution. When $\zeta_{\max} \gtrsim 0.8$, there are two solutions to the turbulent flux parameterization (8), and Algorithm 2 may converge to either solution depending on the initial guess. For the small interval $0.5 \lesssim \zeta_{\max} \lesssim 0.8$, only the desired solution that does not vary with $\zeta_{\max}$ is obtained, and this finding suggests that the value of $\zeta_{\max}$ should fall in this interval to guarantee convergence of Algorithm 2 to the desired solution.

3.5.2 Adaptive selection of limiting parameters

The preceding discussion in Section 3.5.1 suggests that there is no single value of $\zeta_{\max}$ that will ensure the existence of only one solution to the turbulent flux parameterization for all meteorological conditions. For instance, for the meteorological conditions described in Figure 11d, a value of $\zeta_{\max} = 0.6$ is appropriate but would result in obtaining an undesired solution if the same value is used for the meteorological conditions described in Figure 11b.

Instead, we propose utilizing an adaptive stability limiter in which the value of $\zeta_{\max}$ is permitted to vary based on the meteorological conditions. The key idea is to begin with an initial maximum value of $\zeta_{\max}$ and apply Algorithm 2 to obtain a first approximation of the scaling parameters u_*, θ_*, and q_*. If the value of the stability parameter associated with scaling parameters, $\tilde{\zeta}(u_*, \theta_*, q_*; \zeta_{\max})$, is equal to $\zeta_{\max}$, we decrease the value of $\zeta_{\max}$ and

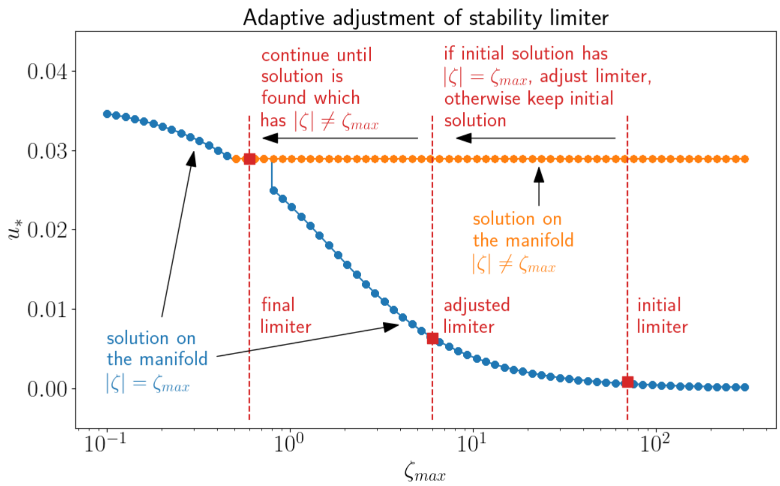

Figure 12: An example of the adaptive stability limiting process. For the initial limiter, two solutions exist – the desired solution which is constant in $\zeta_{\max}$ (orange curve) and the second, undesired solution that lines on the manifold described by $|\tilde{\zeta}| = \zeta_{\max}$ (blue curve). If the desired solution is obtained by Algorithm 3, there is no need to adjust the limiting parameter $\zeta_{\max}$. Otherwise, we incrementally decrease $\zeta_{\max}$ until a solution satisfying $|\tilde{\zeta}| \neq \zeta_{\max}$ is reached. In this example, the process is guaranteed to terminate once $\zeta_{\max}$ falls in the approximate interval $(0.5, 0.8)$. In general, if the process terminates without finding the desired solution, e.g. because it does not exist (see Figure 11c), then we default to the solution obtained from the default E3SM limiting parameter value of $\zeta_{\max} = 10$. A more detailed discussion may be found in Section 3.5.2.

apply Algorithm 2 until scaling parameters are obtained for which $\tilde{\zeta}(u_*, \theta_*, q_*; \zeta_{\max}) \neq \zeta_{\max}$. A visualization of this procedure is provided in Figure 12. The complete turbulent flux algorithm with adaptive stability limiter is presented in Algorithm 3.

Algorithm 3 Modified atmosphere-ocean iteration for uniqueness.

Input: Bulk variables U, $\Delta\theta$, and Δq; damping parameter $\alpha \in (0, 1]$; limiter increment $\zeta_{\text{incr}} > 0$; tolerance `tol`; maximum iterations `maxiter`.

Output: Approximation $(u_*)_n$, $(u_{10N})_n$, $(\theta_*)_n$, and $(q_*)_n$ to the turbulent flux parameterization (19).

procedure RegularizedUniqueIteration(U, $\Delta\theta$, Δq, $\zeta_{\max}$, α, `tol`, `maxiter`)
  Set $\tilde{\zeta}_n = \zeta_{\max}$.
  while $\tilde{\zeta}_n = \zeta_{\max}$ and $\zeta_{\max} > 0$ **do**
    Increment $\zeta_{\max} \leftarrow \max\{\zeta_{\max} - \zeta_{\text{incr}}, 0\}$.
    Call $[(u_*)_n, (\theta_*)_n, (q_*)_n]$ = RegularizedIteration(U, $\Delta\theta$, Δq, $\zeta_{\max}$, α, `tol`, `maxiter`).
    Compute limited stability parameter $\tilde{\zeta}_n = \tilde{\zeta}((u_*)_n, (\theta_*)_n, (q_*)_n; \zeta_{\max})$ according to (7).
  end while

  if $\zeta_{\max} = 0$ **then**
    Set $\zeta_{\max} = 10$.
    Call $[(u_*)_n, (\theta_*)_n, (q_*)_n]$ = RegularizedIteration(U, $\Delta\theta$, Δq, $\zeta_{\max}$, α, `tol`, `maxiter`).
  end if
return $(u_*)_n$, $(\theta_*)_n$, $(q_*)_n$.
end procedure

When there is no desired solution, e.g. the example in Figure 11c, we elect to leave the limiting parameter at its default value of $\zeta_{\max} = 10$. As previously mentioned, this scenario suggests that the underlying assumptions for which the turbulent flux parameterization (8) has been developed have been violated. Addressing this issue is beyond the mathematical analysis presented in this work and we only note its existence here.

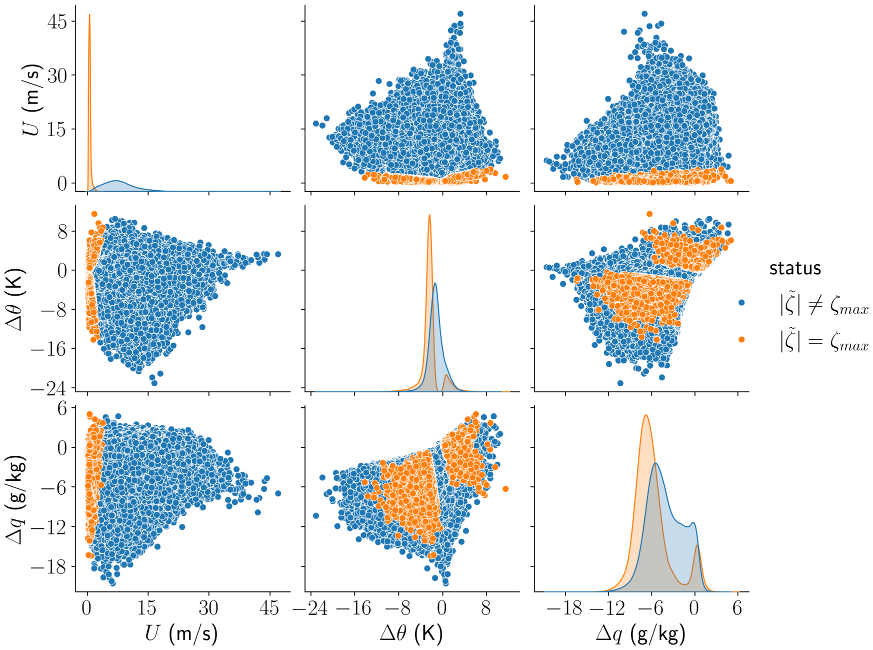

Figure 13: A corner plot similar to Fig. 5 but comparing atmospheric conditions that yield $|\tilde{\zeta}| = \zeta_{\max}$ and those that yield $|\tilde{\zeta}| \neq \zeta_{\max}$.

3.5.3 Occurrence of undesired solutions in E3SM

The preceding discussion highlights the issues associated with the stability limiter (7). In particular, current implementations of ocean-atmosphere turbulent flux algorithms may potentially converge to undesired solutions on the manifold $|\zeta| = \zeta_{\max}$. To better understand the physical conditions producing $|\zeta| = \zeta_{\max}$, we again consider ten years of data from the CTRL simulation. We apply the default Algorithm 1 and categorize each spatial location based on the value of ζ after 100 iterations. Figure 13 shows the distribution of meteorological conditions when $|\zeta| = \zeta_{\max}$ and when $|\zeta| \neq \zeta_{\max}$. The clearest distinction between the two cases is that locations for which $|\zeta| = \zeta_{\max}$ have relatively small wind speeds of less than 2 m/s. Such conditions are most frequent around the Equator, especially across the Indian Ocean, as shown in Figure 14.

4 Climatological impact on E3SM simulations

We perform a pair of 10-year simulations – CTRL and SENS described in Section 2.1 – to investigate the sensitivity of E3SM to the proposed changes in Algorithm 3. For SENS, a tolerance of `tol` $= 10^{-4}$ is used for the stopping criterion with a maximum permissible

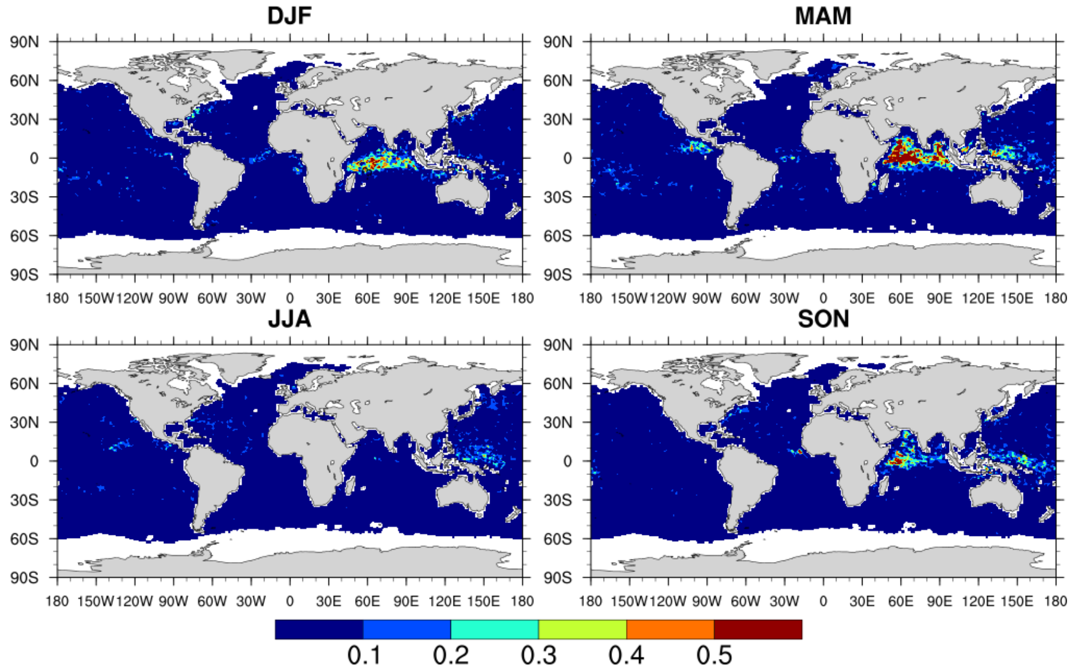

Figure 14: Percentage of days for which $|\tilde{\zeta}| = \zeta_{\max}(= 10)$ in ten years of daily instantaneous output from the CTRL simulation. The condition $|\tilde{\zeta}| = \zeta_{\max}$ indicates that the surface fluxes lie on the manifold of solutions to (19) which vary with $\zeta_{\max}$. Different panels correspond to different seasons. Gray shading indicates land, and white areas are sea ice.

number of iterations `maxiter` $= 2 \times 10^6$; the value of `maxiter` is arbitrarily chosen to be significantly larger than expected to reach the specified tolerance. A C^0 regularization is used to enforce continuity of the exchange coefficient C_{HN} with $\varepsilon_{\text{reg}} = 0.5$. A damping value of $\alpha = 0.08$ is employed in the iteration. Lastly, an initial stability limiting parameter of $\zeta_{\max} = 20$ is used with an increment of $\zeta_{\text{incr}} = 0.25$ in the adaptive limiting process. To determine which differences are statistically significant, a one-sample Student's t-test is performed using monthly mean output data. Since the data are serially correlated, we utilize a revised t-test in which the t statistic is scaled by an effective sample size (Zwiers & von Storch, 1995). A significance level of 0.05 is utilized to determine when the mean of the differences is likely to be non-zero.

The largest effect on latent and sensible heat fluxes occurs in boreal winter (DJF) (right panels of Figure 15). Statistically significant differences in both fluxes cover most of the globe. The largest differences, however, are in the Northern Hemisphere with large increases centered over the North Atlantic. The new algorithm also produces large decreases in latent

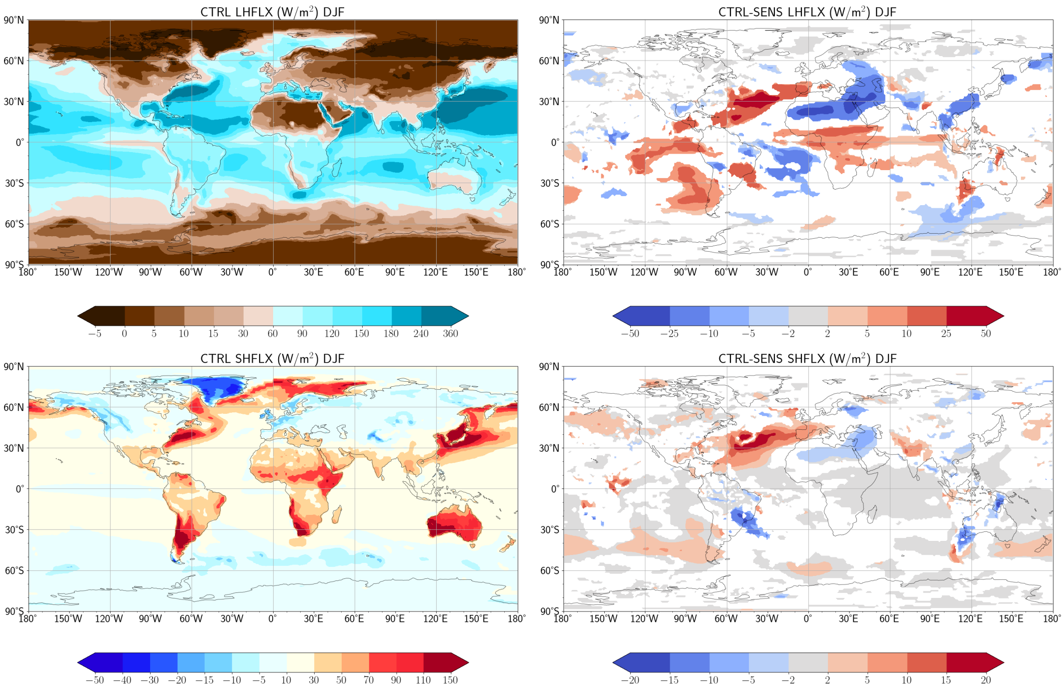

Figure 15: The 10-year mean latent heat flux (top row) and sensible heat flux (bottom row) for the months DJF, as well as the difference between the control and test simulations (right column) in which statistically insignificant differences are masked out in white.

heat flux of similar magnitude over the subtropical deserts of North Africa and the Middle East. These results show that ensuring that the atmosphere-ocean turbulent flux parameterizations are well-posed has a significant impact on Earth system model simulations.

5 Conclusions

We have analyzed the default ocean-atmosphere turbulent flux parameterization in E3SMv2 to determine under which conditions the underlying equations have a unique solution. Our analysis has shown that there are certain physical conditions, mostly encountered in the mid-latitude oceans under stable conditions, for which there is no solution to the underlying equations, and any algorithm attempting to compute surface fluxes from this parameterization will fail to converge. This non-convergence manifests as oscillations of the surface flux iterates and results in a rather large residual error ($>$ 50% on average). Moreover, we have shown that the W. Large & Pond (1982) turbulent flux parameterization does not always yield unique surface fluxes and the use of *ad hoc* limiters on the Obukhov length has a strong influence on the number of solutions. Meteorological conditions that produce non-unique solutions are found mostly in regions with low wind speed near the Equator.

We have introduced two modifications to the W. Large & Pond (1982) algorithm in order to enforce both existence and uniqueness of the computed surface fluxes. These modifications include (i) regularization of discontinuous exchange coefficients which resolves issues with oscillating surface fluxes corresponding to large residual errors, and (ii) adaptive selection of limiter parameters to eliminate multiple solutions. Our analysis also demonstrates the need to exercise caution when applying turbulent flux algorithms globally under conditions for which the underlying assumptions of the algorithm are violated. For instance, in the extreme stability limit as $\zeta \to +\infty$, the assumptions of Monin-Obukhov Similarity Theory are violated, suggesting that the W. Large & Pond (1982) formulation should not be utilized under these conditions.

Sensitivity of E3SMv2's mean climate to these issues of well-posedness was investigated by comparing a 10-year simulations using the default iteration in Algorithm 1 and the regularized iteration in Algorithm 3. The regularized iteration results in statistically significant differences in the model latent and sensible heat fluxes compared to those of the default iteration.

Results in this work utilize a fully converged nonlinear iteration. This is important for ensuring the algorithm attains a specified level of accuracy. While the cost of additional iterations beyond the default of two in the E3SMv2 code is small, we have also demonstrated that techniques such as Anderson acceleration can significantly reduce the added cost of fully converging the iteration.

The analysis in this study provides a framework for future investigation of other ocean-atmosphere flux algorithm options in E3SM such as the COARE (Fairall et al., 2003) and the University of Arizona (UA, Zeng et al., 1998) algorithms. The limiter (7) is also applied in the UA algorithm as implemented in E3SMv2. Furthermore, COARE utilizes limiters for wind gustiness whose effect on uniqueness of the computed surface fluxes has not yet been studied. Additionally, turbulent flux algorithms over sea ice and land share many similarities with the ocean-atmosphere algorithms since they too are based on MOST. They may also include discontinuous exchange coefficients in certain scenarios as well as *ad hoc* use of stability limiters as seen here in the ocean-atmosphere algorithm and will be the subject of future research.

Open Research Section

Model run data corresponding to the CTRL simulation and Python scripts used to generate bifurcation diagrams may be found in Dong et al. (2024a). Model run data corresponding to the SENS simulation may be found in Dong et al. (2024b). A fork of E3SMv2 containing the proposed changes to E3SM's ocean-atmosphere turbulent flux algorithm in Algorithm 3 may be found at Dong (2024).

Acknowledgments

This research used resources of the National Energy Research Scientific Computing Center (NERSC), a U.S. Department of Energy Office of Science User Facility located at Lawrence Berkeley National Laboratory, operated under Contract No. DE-AC02-05CH11231 using NERSC award ASCR-ERCAP0028881.

This work was performed under the auspices of the U.S. Department of Energy by Lawrence Livermore National Laboratory under Contract DE-AC52-07NA27344. LLNL-JRNL-2001306-DRAFT. Pacific Northwest National Laboratory is operated for the U.S. Department of Energy by Battelle Memorial Institute under contract DE-AC06-76RLO1830.

This material is based upon work supported by the U.S. Department of Energy, Office of Science, Office of Advanced Scientific Computing Research (ASCR) and Office of Biological and Environmental Research (BER), Scientific Discovery through Advanced Computing (SciDAC) program, via an ASCR-BER partnership in Earth System Model Development.

The authors would like to thank Sean P. Santos for helpful discussions and feedback in the writing of this manuscript as well as Kezhen Chong for her guidance in post-processing E3SM simulation data. We also thank Arshia Singhal for her initial investigation of the use of Anderson acceleration techniques for computing turbulent fluxes.

References

Anderson, D. G. (1965). Iterative procedures for nonlinear integral equations. *Journal of the ACM (JACM)*, *12*(4), 547–560.

Brunke, M. A., Fairall, C. W., Zeng, X., Eymard, L., & Curry, J. A. (2003). Which Bulk Aerodynamic Algorithms are Least Problematic in Computing Ocean Surface Turbulent Fluxes? *Journal of Climate*, *16*(4), 619 - 635. doi: 10.1175/1520-0442(2003)016⟨0619:WBAAAL⟩2.0.CO;2

Brunke, M. A., Zeng, X., & Anderson, S. (2002). Uncertainties in sea surface turbulent flux algorithms and data sets. *Journal of Geophysical Research: Oceans*, *107*(C10), 5-1-5-21. doi: 10.1029/2001JC000992

Chow, S.-N., & Hale, J. K. (2012). *Methods of bifurcation theory* (Vol. 251). Springer Science & Business Media.

Dong, J. (2024). *E3SMv2 with ocean-atmosphere flux regularization.* GitHub. Retrieved from https://github.com/PAESCAL-SciDAC5/E3SM-fork/tree/maint-2.0_CondiDiag1.0_RHNregularization

Dong, J., Brunke, M. A., Zeng, X., Woodward, C. S., Vogl, C. J., & Wan, H. (2024a, December). *Existence and uniqueness in ocean-atmosphere turbulent flux algorithms in E3SM (pt. 1).* Zenodo. Retrieved from https://doi.org/10.5281/zenodo.14263771 doi: 10.5281/zenodo.14263771

Dong, J., Brunke, M. A., Zeng, X., Woodward, C. S., Vogl, C. J., & Wan, H. (2024b, December). *Existence and uniqueness in ocean-atmosphere turbulent flux algorithms in E3SM (pt. 2).* Zenodo. Retrieved from https://doi.org/10.5281/zenodo.14263844 doi: 10.5281/zenodo.14263844

Fairall, C. W., Bradley, E. F., Hare, J. E., Grachev, A. A., & Edson, J. B. (2003). Bulk Parameterization of Air–Sea Fluxes: Updates and Verification for the COARE Algorithm. *Journal of Climate*, *16*(4), 571 - 591. doi: 10.1175/1520-0442(2003)016⟨0571:BPOASF⟩2.0.CO;2

Gardner, D. J., Guerra, J. E., Hamon, F. P., Reynolds, D. R., Ullrich, P. A., & Woodward, C. S. (2018). Implicit–explicit (IMEX) Runge–Kutta methods for non-hydrostatic atmospheric models. *Geoscientific Model Development*, *11*(4), 1497–1515. doi: 10.5194/gmd-11-1497-2018

Golaz, J.-C., Caldwell, P. M., Van Roekel, L. P., Petersen, M. R., Tang, Q., Wolfe, J. D., ... Zhu, Q. (2019). The DOE E3SM Coupled Model Version 1: Overview and Evaluation at Standard Resolution. *Journal of Advances in Modeling Earth Systems*, *11*(7), 2089-2129. doi: 10.1029/2018MS001603

Harrop, B. E., Ma, P.-L., Rasch, P. J., Neale, R. B., & Hannay, C. (2018). The Role of Convective Gustiness in Reducing Seasonal Precipitation Biases in the Tropical West Pacific. *Journal of Advances in Modeling Earth Systems*, *10*(4), 961-970. doi: 10.1002/2017MS001157

Hindmarsh, A. C., Brown, P. N., Grant, K. E., Lee, S. L., Serban, R., Shumaker, D. E.,

& Woodward, C. S. (2005, September). SUNDIALS: Suite of nonlinear and differential/algebraic equation solvers. *ACM Transactions on Mathematical Software*, *31*(3), 363–396. doi: 10.1145/1089014.1089020

Hurrell, J. W., Holland, M. M., Gent, P. R., Ghan, S., Kay, J. E., Kushner, P. J., ... Marshall, S. (2013). The Community Earth System Model: A Framework for Collaborative Research. *Bulletin of the American Meteorological Society*, *94*(9), 1339 - 1360. doi: 10.1175/BAMS-D-12-00121.1

Isaacson, E., & Keller, H. B. (1994). *Analysis of numerical methods.* Courier Corporation.

Large, W., & Pond, S. (1982). Sensible and latent heat flux measurements over the ocean. *Journal of physical Oceanography*, *12*(5), 464–482. doi: 10.1175/1520-0485(1982)012⟨0464:SALHFM⟩2.0.CO;2

Large, W. B. (2006). Surface Fluxes for Practitioners of Global Ocean Data Assimilation. In E. P. Chassignet & J. Verron (Eds.), *Ocean weather forecasting: An integrated view of oceanography* (pp. 229–270). Dordrecht: Springer Netherlands. doi: 10.1007/1-4020-4028-8_9

Large, W. G., & Caron, J. M. (2015). Diurnal cycling of sea surface temperature, salinity, and current in the CESM coupled climate model. *Journal of Geophysical Research: Oceans*, *120*(5), 3711-3729. doi: 10.1002/2014JC010691

Large, W. G., & Pond, S. (1981). Open Ocean Momentum Flux Measurements in Moderate to Strong Winds. *Journal of Physical Oceanography*, *11*(3), 324 - 336. doi: 10.1175/1520-0485(1981)011⟨0324:OOMFMI⟩2.0.CO;2

Ma, P.-L., Harrop, B. E., Larson, V. E., Neale, R. B., Gettelman, A., Morrison, H., ... Leung, L. R. (2022). Better calibration of cloud parameterizations and subgrid effects increases the fidelity of the E3SM Atmosphere Model version 1. *Geoscientific Model Development*, *15*(7), 2881–2916. doi: 10.5194/gmd-15-2881-2022

Monin, A. S., & Obukhov, A. M. (1954). Basic laws of turbulent mixing in the surface layer of the atmosphere. *Contrib. Geophys. Inst. Acad. Sci. USSR*, *24*(151), 163-187.

Optis, M., Monahan, A., & Bosveld, F. C. (2016). Limitations and breakdown of Monin–Obukhov similarity theory for wind profile extrapolation under stable stratification. *Wind Energy*, *19*(6), 1053-1072. doi: 10.1002/we.1883

Ortega, J. M., & Rockoff, M. L. (1966). Nonlinear difference equations and Gauss-Seidel type iterative methods. *SIAM Journal on Numerical Analysis*, *3*(3), 497–513.

Reeves Eyre, J. E. J., Zeng, X., & Zhang, K. (2021). Ocean Surface Flux Algorithm Effects on Earth System Model Energy and Water Cycles. *Frontiers in Marine Science*, *8*. doi: 10.3389/fmars.2021.642804

Vogl, C. J., Steyer, A., Reynolds, D. R., Ullrich, P. A., & Woodward, C. S. (2019). Evaluation of Implicit-Explicit Additive Runge-Kutta Integrators for the HOMME-NH Dynamical Core. *Journal of Advances in Modeling Earth Systems*, *11*(12), 4228-4244. doi: 10.1029/2019MS001700

Wan, H., Rasch, P. J., Taylor, M. A., & Jablonowski, C. (2015). Short-term time step convergence in a climate model. *Journal of Advances in Modeling Earth Systems*, *7*(1), 215-225. doi: 10.1002/2014MS000368

Wan, H., Zhang, K., Rasch, P. J., Larson, V. E., Zeng, X., Zhang, S., & Dixon, R. (2022). Condidiag1.0: a flexible online diagnostic tool for conditional sampling and budget analysis in the e3sm atmosphere model (eam). *Geoscientific Model Development*, *15*(8), 3205–3231. doi: 10.5194/gmd-15-3205-2022

Wan, H., Zhang, K., Vogl, C. J., Woodward, C. S., Easter, R. C., Rasch, P. J., . . . Wang, H. (2024). Numerical coupling of aerosol emissions, dry removal, and turbulent mixing in the E3SM Atmosphere Model version 1 (EAMv1) – Part 1: Dust budget analyses and the impacts of a revised coupling scheme. *Geoscientific Model Development*, *17*(3), 1387–1407. doi: 10.5194/gmd-17-1387-2024

Wan, H., Zhang, S., Rasch, P. J., Larson, V. E., Zeng, X., & Yan, H. (2021). Quantifying and attributing time step sensitivities in present-day climate simulations conducted with EAMv1. *Geoscientific Model Development*, *14*(4), 1921–1948. doi: 10.5194/gmd-14-1921-2021

Xie, S., Lin, W., Rasch, P. J., Ma, P.-L., Neale, R., Larson, V. E., . . . Zhang, Y. (2018). Understanding Cloud and Convective Characteristics in Version 1 of the E3SM Atmosphere Model. *Journal of Advances in Modeling Earth Systems*, *10*(10), 2618-2644. Retrieved from https://agupubs.onlinelibrary.wiley.com/doi/abs/10.1029/2018MS001350 doi: 10.1029/2018MS001350

Zeng, X., & Beljaars, A. (2005). A prognostic scheme of sea surface skin temperature for modeling and data assimilation. *Geophysical Research Letters*, *32*(14). doi: 10.1029/2005GL023030

Zeng, X., Zhao, M., & Dickinson, R. E. (1998). Intercomparison of Bulk Aerodynamic Algorithms for the Computation of Sea Surface Fluxes Using TOGA COARE and TAO Data. *Journal of Climate*, *11*(10), 2628 - 2644. doi: 10.1175/1520-0442(1998)011⟨2628:

IOBAAF⟩2.0.CO;2

Zhang, S., Vogl, C. J., Larson, V. E., Bui, Q. M., Wan, H., Rasch, P. J., & Woodward, C. S. (2023). Removing Numerical Pathologies in a Turbulence Parameterization Through Convergence Testing. *Journal of Advances in Modeling Earth Systems*, *15*(5), e2023MS003633. doi: 10.1029/2023MS003633

Zwiers, F. W., & von Storch, H. (1995). Taking Serial Correlation into Account in Tests of the Mean. *Journal of Climate*, *8*(2), 336 - 351. doi: 10.1175/1520-0442(1995)008⟨0336:TSCIAI⟩2.0.CO;2